Received: 11 August 2023 | Revised: 22 November 2023 | Accepted: 27 November 2023

IET Generation, Transmission & Distribution

DOI: 10.1049/gtd2.13077

The Institution of Engineering and Technology WILEY

ORIGINAL RESEARCH

Enhanced sliding mode controller design via meta-heuristic algorithm for robust and stable load frequency control in multi-area power systems

Anh-Tuan Tran[1] | **Minh Phuc Duong**[1] | **Nhat Truong Pham**[2] | **Jae Woong Shim**[3]

[1]Faculty of Electrical and Electronics Engineering, Ton Duc Thang University, Ho Chi Minh City, Vietnam

[2]Department of Integrative Biotechnology, College of Biotechnology and Bioengineering, Sungkyunkwan University, Suwon, Republic of Korea

[3]Department of Electrical Engineering, Sangmyung University, Seoul, Republic of Korea

Correspondence
Jae Woong Shim, Department of Electrical Engineering, Sangmyung University, Seoul, Republic of Korea.
Email: jaewshim@smu.ac.kr

Funding information
National Research Fund of Korea, Grant/Award Number: 2021R1C1C1012806; Korea Electric Power Corporation, Grant/Award Number: R21XO02-2

Abstract

This article introduces a novel approach named HBA-dHoSMO, which combines a continuous decentralized higher-order sliding mode controller-based observer (dHoSMO) with the honey badger algorithm (HBA), specifically designed for load frequency control in multi-area power systems (MAPSs). Traditional sliding mode controllers (SMCs) employed in load frequency control of MAPSs often face challenges related to chattering and oscillations, leading to decreased robustness and stability. Additionally, tuning the parameters for these SMC designs to achieve optimal performance in MAPSs can be challenging. The HBA-dHoSMO is proposed to address the issues of chattering and oscillations, while the optimal parameters for SMC design are obtained using HBA. The stability analysis of the entire system is conducted using linear matrix inequality and the Lyapunov stability theory, affirming the reliability and feasibility of the approach. A comprehensive set of case studies is performed under various configurations and conditions. Additionally, particle swarm optimization and tuna swarm optimization, in conjunction with SMC-based and proportional–integral–derivative controllers, are examined for performance comparison. Simulation results demonstrate the superior performance of the proposed controller across all case studies. This is evidenced by the lowest integral time absolute error values recorded as 0.0133, 6.45×10^{-4}, and 0.0167 for single-, two-, and three-area power systems, respectively.

1 | INTRODUCTION

1.1 | Background

Power system (PS) operation schemes get more complicated due to the variability of load demand and renewable generation, the complexity of electrical components, plant uncertainties, and especially the exchange of electricity between neighbour areas. PS control schemes are employed to maintain the PS in a stable state, and load frequency control (LFC) is an important control issue in wide-area PS operations. The main requirements of the grid code regarding stability are the ability to remain normal operation in presence of load disturbances and generation uncertainties. That means the system frequency is maintained in the desired values [1, 2]. There are two major objectives of LFC including keeping the frequency of each area in the desired range and interchanged power between nearby areas within the allowable limit [3–5].

1.2 | Literature review

In the past decade, a range of control strategies have been developed for LFC in PS. These strategies encompass traditional methods like the proportional–integral–derivative (PID) technique, as well as advanced techniques including sliding mode control (SMC) and other sophisticated approaches such as meta-heuristic and optimization techniques. This section offers a brief summary of each of these methods.

In the conventional approach, there have been a lot of proposed controllers designed PID technique for LFC in PS. Specifically, Nosratabadi et al. [6] employed the Grasshopper

optimization algorithm to design a new predictive functional modified PID controller, aiming to improve the system performance of an integrated redox flow battery (RFB) multi-source multi-area PS. This new controller demonstrated competitiveness compared to other optimization methods in mitigating various possible disturbances. Sharma et al. [7] performed a comparative analysis of LFC designs using the Jaya optimization algorithm to fine-tune parameters for various conventional controllers, including integral (I), proportional–integral (PI), PID, integral–derivative (ID), and integral–double-derivative (IDD) controllers. This assessment was conducted on a two-area photovoltaic-thermal system, integrated with an ultracapacitor and RFB in each zone of the photovoltaic-thermal system. In [8], an innovative integral derivative-tilted controller was introduced for a two-area PS by modifying the structure of the tilted integral derivative controller using the Archimedes optimization algorithm. Notably, this approach enhanced the system performance of the PS across various system conditions. In [9], a dragonfly search algorithm (DSA) integrated cascade controller was designed for single- and multi-area PS by combining (1+PD) and PID controllers. It was proven to outperform other approaches under various system conditions. However, since the application of DSA to address the LFC problem is lacking, further examination and analysis are still required for this approach. Additionally, in the domain of frequency regulation for micro-grid systems, optimization-based fuzzy PID controllers were proposed [10, 11]. In [12], the authors proposed a physics-inspired atom search optimization (ASO) algorithm to tune the parameters of a fractional order PID (FOPID) controller for automatic LFC of interconnected hybrid PS integrating renewable energy sources (wind and solar) and energy storage devices (aqua electrolyzer, fuel cell, and electric vehicle). The ASO-tuned FOPID controller demonstrates superior transient and steady-state responses compared to other controllers, and its robustness is validated against changes in renewable energy generation and system parameters. This proposed controller's effectiveness is further verified by comparing its performance with other literature works, and its real-time applicability is validated in hardware-in-the-loop simulation using a real-time digital simulator. Veerasamy et al. [13] offered a comprehensive approach to automatic LFC in a multi-source hybrid PS, integrating conventional and renewable energy sources. The use of cascade PI-PD control with PSO-gravitational search algorithm (GSA) optimization demonstrates significant performance improvements over other classical controllers, highlighting its potential in enhancing frequency stability and robustness in real-world PSs. The stability analysis and comparison with other artificial intelligence (AI) methods add further credibility to their proposed approach. Recently, several methods for LFC in PS have been reported in the literature [14–17]. For instance, control techniques, soft computing algorithms, and energy storage technologies applicable to LFC in PS were summarized in [14]. In [17], the authors presented an up-to-date and state-of-the-art report on the challenges and future directions of automatic generation control (AGC) and LFC in both conventional and renewable energy-based PS. In the works of Darvish et al. [18–20], various optimization-based and intelligent techniques employing fractional-order-PID controllers were developed for AGC in PSs. These methods include type-2 fuzzy logic, multi-objective-based optimizations utilizing algorithms such as ant lion optimizer, particle swarm optimization (PSO), and bees algorithm, as well as non-dominated sorting genetic algorithm II. In contrast to LFC, Eke et al. [21] introduced heuristic optimization controllers based on PID for automatic voltage regulation in PSs. This illustrates the diverse applications of PID-based control methods within the PS domain. Additionally, intelligent control techniques based on PI controllers, including fuzzy logic, AI, model predictive control, genetic algorithms, adaptive neuro-fuzzy inference systems, and Harris Hawks optimization (HHO), have been employed in various PS applications, including wind energy grid connection systems [22–28]. More recently, the honey badger algorithm (HBA) was introduced by Hashim et al. [29] that outperformed other meta-heuristic algorithms based on the CEC'17 serial benchmark functions. As a result, several approaches have been employed HBA to tune the optimal parameters for PID-based controllers for LFC in PSs [30–33].

SMC is well-known as one of the robust variable structure controls that help the system obtain high performance. Besides, SMC is also non-sensitive to the change of the system parameters and load disturbances. Thus, SMC is widely applied in many different fields such as electrical vehicles [34], non-linear systems [35], and PSs [36–40]. However, the old-fashion SMC exists some limitations, so a lot of improved SMC schemes have been suggested with the various sliding surfaces [41–44]. In [41], a first-order SMC is suggested to manage load frequency in multi-area power systems (MAPS) under matched and mismatched uncertainties, which still suffer from the chattering phenomenon. Therefore, in [42], the authors designed the adaptive integral higher-order SMC to free chattering and obtain a smooth control signal for MAPS under varying operating conditions. More recently, Alyoussef and Kaya [45] introduced an innovative non-singular terminal SMC method, incorporating a novel adaptive reaching law integrated with a fractional disturbance observer. This approach was developed to tackle singularity and chattering issues while effectively eliminating severe and time-varying disturbances in PSs. Although this controller is quite robust and stable, this approach is not very reliable, because of the high dependence on the exact measurement of system state variables (SSVs) by the sensors. Evidently, in a large-scale PS, accurately measuring all system states is not easy. To handle the aforementioned problems, many studies have utilized SMC combined with an observer-based LFC of MAPS, as suggested in these studies [43, 44, 46–49]. But these researchers only used a centralized LFC approach. Clearly, the decentralized LFC approach is more viable than the centralized one, because this just uses state variables information in the local area to manage the frequency fluctuation. In addition, to maximize the performance of the controller, many researchers have combined SMC with meta-heuristic algorithms. In this regard, to obtain an optimal result, the parameters of the SMC controller should be determined by optimization algorithms [50–53]. In [51], a Black Hole optimization is applied for SMC to tune the coefficients of model-free

technique regulated load frequency in a stand-alone microgrid with time delay. In [52], the authors suggested SMC for LFC in Great Britain PS integrated bees algorithm under load disturbances and parameter uncertainties. Zhang et al. [54] presented a novel hybrid control strategy that combines PSO, SMC, and fuzzy PID control to stabilize an open-loop unstable magnetic levitation system. Their proposed method effectively addresses the chattering phenomenon of SMC and demonstrates strong robustness against external disturbances and state variable crossing. Once again, in [53], an SMC is continuously designed for LFC using grey wolf optimization to select the parameters of the controller to achieve optimal performance. Although the performance of these schemes in studies [51–53] are exploited to the maximum by the algorithms, it is still restricted due to the controllers being designed based on first-order SMC.

1.3 | Research gap and motivation

Recent studies highlight the prevalent use of PID-based and SMC-based controllers in LFC for PSs. Moreover, in efforts to enhance performance and streamline the parameter selection process for these methods, various meta-heuristic algorithms and intelligent control techniques have been explored. These include AI, ASO, DSA, HHO, PSO, GSA, fuzzy logic, and HBA. Notably, HBA has emerged as a cutting-edge meta-heuristic algorithm. Despite its application in optimizing parameters for PID-based controllers, no previous research has utilized it to optimize parameters for SMC-based controllers in LFC for PSs. This research gap motivated our study.

1.4 | Challenges

Although SMC has been proven efficiently and robust for load frequency regulation of the PSs from the literature, there are still several challenges in designing the SMC for LFC in MAPS that can be listed as follows:

- Nonlinear and uncertain dynamics, such as changing loads, load disturbances, and renewable energy integration.
- Conventional and low-order SMCs can suffer from chattering phenomenon. Consequently, the PSs can lead to reduced efficiency and stability.
- Maintaining the stability of the SMC under varying operating conditions and disturbances is challenging, especially in MAPS.
- Lastly, tuning the parameters for SMC design to obtain the optimal performance in MAPS can be also challenging.

1.5 | Objective and contribution

This article aims to solve the challenges in designing SMC for LFC in MAPS. Specifically, a continuous decentralized higher-order SMC-based observer (dHoSMO) is designed to eliminate the chattering phenomenon in MAPS. Subsequently, the latest meta-heuristic algorithm, e.g. HBA [29], is applied to obtain the optimal parameters for such SMC design. To validate the robustness and stability of the proposed controller, several case studies are conducted with different configurations and conditions. Simulation results reveal that by combining dHoSMO with the HBA, the proposed controller becomes much more robust and stable.

The major contributions of this article are listed as follows:

- The continuous decentralized higher-order SMC rule based on the estimated local SSVs is developed to improve system performance by eliminating the oscillating and chattering issues.
- Three meta-heuristic algorithms are assessed, namely HBA, PSO [55], and tuna swarm optimization (TSO) [56], to obtain the optimal parameters for SMC design for different case studies and conditions. To the best of our knowledge, this is the first time HBA and TSO are investigated to obtain the optimal parameters for SMC design.
- The HBA technique was proven that its performance surpassed almost state-of-the-art meta-heuristic algorithms. Interestingly, combining dHoSMO with the HBA technique obtains the best performance in this study too.
- A novel linear matrix inequality (LMI) technique based on actual and estimated SSVs is established to prove the entire stability of MAPS based on Lyapunov stability theory.
- Simulation results indicate that the proposed approach is reliable against system parameter uncertainties and satisfactorily work with large-scale practice PS.

1.6 | Article organization

The structure of the article is organized as follows: Section 2 formulates the model for the interconnected MAPS. In Section 3, the design and stability analysis of the state observer-based high-order SMC are presented. The applied HBA is detailed in Section 4. Section 5 provides insights into the implementation of the meta-heuristic algorithms for the dHoSMO controller design problem. Section 6 delves into the analysis and simulation results. Finally, Section 7 concludes this study and suggests avenues for future work.

2 | THE INTERCONNECTED MULTI-AREA POWER SYSTEM MODELLING

In this research, the LFC model is designed with the control system, resources, and loads, which perform a significant role in determining PS reliability. The detailed model of single-area power system (SAPS) and /th area in MAPS are both depicted in Figure 1 as [37, 40, 41, 57, 58]. To reduce frequency variation, each area system in the diagram is equipped with the dHoSMO method integrated with the HBA technique. From Figure 1, the

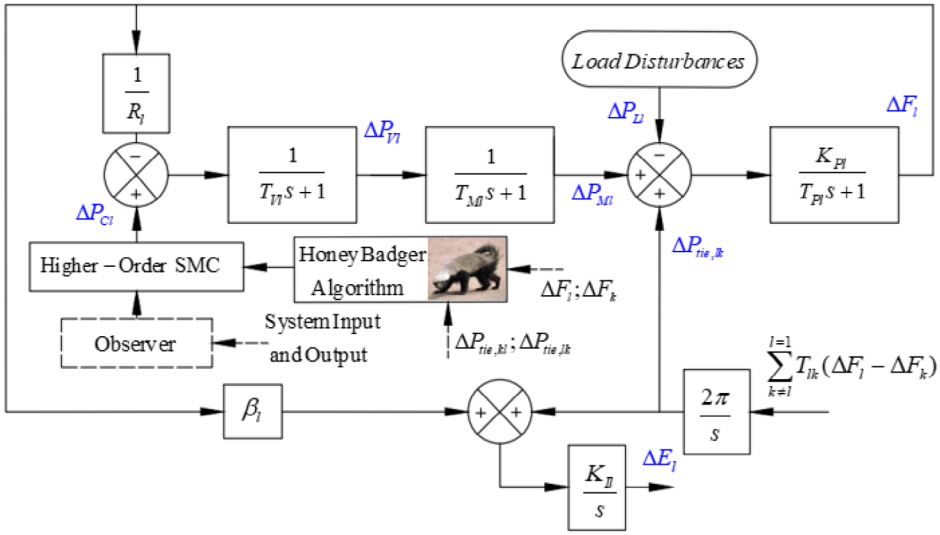

FIGURE 1 Block diagram of the lth area of MAPS.

dynamic equations in the lth area model are deduced as the frequency variation is expressed in Equation (1). The mechanic's power variation is given in Equation (2), and the valve position variation is displayed in Equation (3). The area control error is presented in Equation (4), and the rotor angle variation is shown in Equation (5).

$$\Delta\dot{F}_l(t) = -\frac{1}{T_{Pl}}\Delta F_l(t) + \frac{K_{Pl}}{T_{Pl}}\Delta P_{Ml}(t) - \frac{K_{Pl}}{T_{Pl}}\Delta P_{Ll}(t) + \frac{K_{Pl}}{T_{Pl}2\pi}\sum_{l=1,l\neq k}^{N} T_{lk}[\Delta\delta_l(t) - \Delta\delta_k(t)] \quad (1)$$

$$\Delta\dot{P}_{Ml}(t) = -\frac{1}{T_{Ml}}\Delta P_{Ml}(t) + \frac{1}{T_{Ml}}\Delta P_{Vl}(t) \quad (2)$$

$$\Delta\dot{P}_{Vl}(t) = -\frac{1}{T_{Vl}R_l}\Delta F_l(t) - \frac{1}{T_{Vl}}\Delta P_{Vl}(t) + \frac{1}{T_{Vl}}\Delta P_{Cl}(t) \quad (3)$$

$$\Delta\dot{E}_l(t) = K_{Il}\beta_l\Delta F_l(t) + \frac{K_{Il}}{2\pi}\sum_{l=1,l\neq k}^{N} T_{lk}[\Delta\delta_l(t) - \Delta\delta_k(t)] \quad (4)$$

$$\Delta\dot{\delta}_l(t) = 2\pi\Delta F_l(t) \quad (5)$$

where $\Delta F_l(t)$ is frequency deviation of lth area, $\Delta P_{Ml}(t)$ is gate/valve position change of lth area, $\Delta P_{Vl}(t)$ is mechanical power deviation of lth area, $\Delta E_l(t)$ is area control error of lth area, $\Delta\delta_l(t)$ is rotor angle deviation of lth area, $\Delta P_{Cl}(t)$ is control signal deviation of lth area; T_{Pl} is power system time constant, T_{Ml} is steam time constant, T_{Vl} is governor time constant, T_{lk} is tie-line coefficient, $K_{Pl}, R_l, K_{Il}, \beta_l$ are PS gains; and N is total number of areas.

According to Equations (1)–(5), the dynamic equations can be defined in state-space form in Equation (6).

$$\dot{x}_l(t) = A_l x_l(t) + B_l u_l(t) + C_{lk}x_k(t) + D_l\psi_l(t)2 \quad (6)$$

Then, the associated matrices and vectors of MAPS are given below

$$x_l(t) = [\Delta F_l(t) \quad \Delta P_{Ml}(t) \quad \Delta P_{Vl}(t) \quad \Delta E_l(t) \quad \Delta\delta_l(t)]^T \quad (7)$$

$$u_l(t) = [\Delta P_{Cl}(t)]^T \quad (8)$$

and

$$\omega_l(t) = [\Delta P_{Ll}(t)]^T \quad (9)$$

where $x_l(t)$ is state vector of lth area and $x_k(t) \in R^{n_k}$ is the state vector of neighbouring control areas, $u_l(t)$ is control vector of lth area, and $\omega_l(t)$ is disturbance vector of lth area; A_l is state-space variable matrix, B_l is input control matrix, C_l is associated matrix between nearby areas, and D_l is input disturbance matrix

From the above differential equations, we can determine the matrices

$$A_l = \begin{bmatrix} \frac{1}{T_{Pl}} & \frac{K_{Pl}}{T_{Pl}} & 0 & 0 & -\frac{K_{Pl}}{T_{Pl}2\pi}T_{lk} \\ 0 & -\frac{1}{T_{Tl}} & \frac{1}{T_{Tl}} & 0 & 0 \\ -\frac{1}{T_{Vl}R_l} & 0 & -\frac{1}{T_{Vl}} & 0 & 0 \\ K_{Il}\beta_l & 0 & 0 & 0 & \frac{K_{Il}}{2\pi}T_{lk} \\ 2\pi & 0 & 0 & 0 & 0 \end{bmatrix} \quad (10)$$

$$B_l = \begin{bmatrix} 0 & 0 & \frac{1}{T_{Vl}} & 0 & 0 \end{bmatrix}^T \quad (11)$$

$$C_{lk} = \begin{bmatrix} 0 & 0 & 0 & 0 & \frac{K_{Pl}}{T_{Pl}2\pi}T_{lk} \\ 0 & 0 & 0 & 0 & 0 \\ 0 & 0 & 0 & 0 & 0 \\ 0 & 0 & 0 & 0 & -\frac{K_{Il}}{2\pi}T_{lk} \\ 0 & 0 & 0 & 0 & 0 \end{bmatrix} \tag{12}$$

$$D_l = \begin{bmatrix} -\frac{K_{Pl}}{T_{Pl}} & 0 & 0 & 0 & 0 \end{bmatrix}^T \tag{13}$$

In the actual MAPS, the precise measurement of the component values is incapable due to the operating point constantly changing by the varying load and others. Hence, all parameters can be estimated or approximated. Also, Equation (6) is updated as Equation (14).

$$\begin{aligned} \dot{x}_l(t) &= \bar{A}_l x_l(t) + \bar{B}_l u_l(t) + \bar{C}_{lk} x_k(t) + \bar{D}_l \psi_l(t) \\ &= A_l x_l(t) + B_l u_l(t) + C_{lk} x_k(t) + \omega_l(t) \end{aligned} \tag{14}$$

where $\bar{A}_l = A_l + \Delta A_l$, $\bar{B}_l = B_l + \Delta B_l$, $\bar{C}_l = C_l + \Delta C_l$, $\bar{D}_l = D_l + \Delta D_l$, and the unknown matrices ΔA_l, ΔB_l, ΔC_l, and ΔD_l denote system variations, the matrices A_l, B_l, C_{lk}, and D_l are the nominal values; and $\omega_l(t)$ is called the total disturbances which can be estimated as in Equation (15) below.

$$\omega_l(t) = \Delta A_l x_l(t) + \Delta B_l u_l(t) + \Delta C_{lk} x_k(t) + \bar{D}_l \psi_l(t) \tag{15}$$

In the ideal scenario, some assumptions and lemmas are presented in this part to describe the stability and feasibility of the MAPS-based LFC strategies under certain conditions.

Assumption 1. If the matrix $[A_l, B_l]$ is controllable, $\Delta A_l(t)$ and $\Delta B_l(t)$ can be estimated.

Assumption 2. The pair of matrices $[A_l, F_l]$ is observable.

Lemma 1 [44]. *Let* X *and* Y *are realistic matrices with appropriate dimensions then, for any scalar* $\mu > 0$*, the following matrix inequality achieve*

$$X^T Y + Y^T X \le \mu X^T X + \mu^{-1} Y^T Y \tag{16}$$

Lemma 2 [44]. *If the matrix*

$$\begin{bmatrix} P(x) & R(x) \\ R^T(x) & Q(x) \end{bmatrix} > 0 \tag{17}$$

where $P(x) = P^T(x)$, $Q(x) = Q^T(x)$, and $R(x)$ which depends on x. Therefore, $P(x) - R(x)Q^{-1}(x)R^T(x) > 0$ and $Q(x) > 0$

3 | STATE OBSERVER BASED ON HIGHER-ORDER SMC

The traditional first-order SMC has a significant drawback of high-frequency oscillation caused by fast switch control near the sliding surface (chattering phenomenon). Besides, higher-order SMC brings up superior performance with better tracking accuracy, reduced steady-state errors, and improved disturbance rejection. Especially, this method also can effectively suppress chattering and improve control smoothness compared to first-order SMC. Moreover, the state observer is known for accurately estimating all SSV values based on system output and input signal. Hence, this article proposes a higher-order SMC based on a state observer for local LFC-MAPS. Then, using the estimated SSVs, a higher-order SMC strategy can be implemented to improve the closed-loop system transient performance by eliminating the oscillating and chattering issues.

3.1 | Design of state observer

The designed control systems in studies [37, 42, 43] assumed that all SSVs were available for feedback. However, all SSVs are not available for feedback in practice. Furthermore, the PS structure is highly complex, and direct measurement from sensors of all SSVs in an interconnected PS does not have cost-effectiveness and feasible implementation. Due to those reasons, we must estimate SSVs; thus, the state observer is implemented based on the previous study [59], and explained in this section. The state-space model of state observer based on the lth area model as shown in Equation (14) is illustrated as Equation (18).

$$\begin{aligned} \dot{\hat{x}}_l(t) &= (A_l - L_l F_l)\hat{x}_l(t) + B_l u_l(t) + C_{lk}\hat{x}_k(t) + L_l y_l(t) \\ \hat{y}_l(t) &= F_l \hat{x}_l(t) \end{aligned} \tag{18}$$

where $\hat{x}_l(t) \in R^{n_l}$ and $\hat{x}_k(t) \in R^{n_k}$ is estimated state vector in lth and kth areas respectively, $\hat{y}_l(t)$ is estimated output vector, F_l is output matrix.

According to assumptions 1 and 2, dual systems mentioned in Equations (14) and (18), respectively, are completely controllable and observable. Then, we designed observer gain (H_l) via the pole placement method [59] which causes the eigenvalues $(A_l^T - C_l^T H_l)$ to be placed in predefined locations in the negative hyperplane. The matrix observer gains (L_l) can be chosen by employing the following: $L_l = H_l^T$.

3.2 | Design of higher-order sliding surface based on estimated local SSVs of the state observer

Due to the non-linear characteristics of the realistic system, the difference between the real system and the designed model exists due to dynamic characteristic variations during the PS

operation; thus, the exact calculation of a realistic system model is almost impossible.

The SMC technique is well-known as a robust control method and its design is not based on an exact system model. Hence, it is appropriate to control non-linear systems with external disturbances and plant uncertainties. By applying a designed control law, the system trajectory will be driven to an integral sliding surface [41] and sliding manifold [44] with any initial condition and keep it thereafter. To demonstrate the system performance and robustness under disturbances during the reaching phase, we suggest the new integral sliding surface for the MAPS as Equation (19)

$$\sigma_l\left[\hat{x}_l(t)\right] = \varepsilon_{l1} G_l \hat{x}_l(t) - \varepsilon_{l2} \int_0^t G_l(\mathcal{A}_l - B_l K_l)\hat{x}_l(\tau)\mathrm{d}\tau \quad (19)$$

where ε_{l1} and ε_{l2} are the positive constants chosen by meta-heuristic algorithm, G_l, K_l are the designed matrices. G_l is selected to secure invertible matrix ($G_l B_l$), and K_l is designed by using pole placement technique [59] which causes the eigenvalues $(\mathcal{A}_l - B_l K_l)$ to be chosen in the locations in the negative hyperplane.

Differentiating $\sigma_l[\hat{x}_l(t)]$ in Equation (19) following time and combining with Equation (18), then

$$\begin{aligned}\dot{\sigma}_l\left[\hat{x}_l(t)\right] &= \varepsilon_{l3} G_l \mathcal{A}_l \hat{x}_l(t) + \varepsilon_{l1} G_l B_l u_l(t) + \varepsilon_{l1} G_l C_{lk} \hat{x}_k(t) \\ &\quad + \varepsilon_{l1} G_l L_l[y_l(t) - \hat{y}_l(t)] + \varepsilon_{l2} G_l B_l K_l \hat{x}_l(t) \quad (20)\end{aligned}$$

where ε_{l3} is the value differences between ε_{l2} and ε_{l1} (i.e. $\varepsilon_{l3} = \varepsilon_{l2} - \varepsilon_{l1}$).

So, the setting $\dot{\sigma}_l[\hat{x}_l(t)] = \sigma_l[\hat{x}_l(t)] = 0$, the equivalent control is defined as Equation (21).

$$\begin{aligned}u_l^{eq}(t) &= -(\varepsilon_{l1} G_l B_l)^{-1}\left[\varepsilon_{l3} G_l \mathcal{A}_l \hat{x}_l(t) + \varepsilon_{l1} G_l C_{lk} \hat{x}_k(t)\right. \\ &\quad \left. + \varepsilon_{l1} G_l L_l[y_l(t) - \hat{y}_l(t)] + \varepsilon_{l2} G_l B_l K_l \hat{x}_l(t)\right] \quad (21)\end{aligned}$$

Remark 1. A higher-order SMC approach is designed for the MAPS to eliminate the oscillating and chattering phenomena in the first-order SMC. The main objective of the suggested approach is to affect the high order derivative of the sliding variables $\dot{\sigma}_l[\hat{x}_l(t)]$.

For dHoSMO method, the sliding manifold [44] $\dot{S}_l[\hat{x}_l(t)]$ is design as Equation (22)

$$S_l\left[\hat{x}_l(t)\right] = \dot{\sigma}_l\left[\hat{x}_l(t)\right] + Z_l \sigma_l\left[\hat{x}_l(t)\right] \quad (22)$$

where $Z_l > 0$ is chosen by a meta-heuristic algorithm. Differentiating Equation (22) and substituting Equation (20) we obtain

$$\begin{aligned}&\dot{S}_l\left[\hat{x}_l(t)\right] \\ &= \varepsilon_{l3} G_l \mathcal{A}_l \dot{\hat{x}}_l(t) + \varepsilon_{l1} G_l B_l \dot{u}_l(t) + \varepsilon_{l1} G_l C_{lk} \dot{\hat{x}}_k(t) \\ &\quad + \varepsilon_{l2} G_l B_l K_l \dot{\hat{x}}_l(t) + \varepsilon_{l1} G_l L_l[\dot{y}_l(t) - \dot{\hat{y}}_l(t)] + Z_l \dot{\sigma}_l\left[\hat{x}_l(t)\right] \quad (23)\end{aligned}$$

Based on the explanation of sliding manifold, the continuous dHoSMO controller is designed for LFC of MAPS to be given as follows

$$\begin{aligned}u_l^{HO}(t) = \dot{u}_l(t) &= -(\varepsilon_{l1} G_l B_l)^{-1}\left[\varepsilon_{l3} G_l \mathcal{A}_l \dot{\hat{x}}_l(t)\right. \\ &\quad + \varepsilon_{l1} G_l C_{lk} \dot{\hat{x}}_k(t) + \varepsilon_{l1} G_l L_l[\dot{y}_l(t) - \dot{\hat{y}}_l(t)] \\ &\quad + \varepsilon_{l2} G_l B_l K_l \dot{\hat{x}}_l(t) + Z_l \dot{\sigma}_l[\hat{x}_l(t)] \\ &\quad \left. + \delta_l sat\{S_l[\hat{x}_l(t)]\}\right] \quad (24)\end{aligned}$$

where

$$\mathrm{sat}\{S_l[\hat{x}_l(t)]\} = \begin{cases} \mathrm{sign}\{S_l[\hat{x}_l(t)]\} & \text{if } \|S_l\| > \Phi_l \\ \dfrac{\dot{S}_l[\hat{x}_l(t)]}{\Phi_l} & \text{others} \end{cases} \quad (25)$$

and $\delta_l > 0$ is the control energy chosen by the meta-heuristic algorithm. From the above method, the frequency regulation based on state observer can be implemented for better results.

3.3 | Reachability analysis

For the MAPS, to design the SMC and drive the system state trajectories to the sliding manifold, the reaching condition [41] for each area need to meet Proof of Theorem 1.

Theorem 1. *Considering the closed loop of the MAPS in Equation (14) with the continuous dHoSMO controller in Equation (24). Then, every system trajectory is directly driven to the sliding manifold and once this trajectory reaches the sliding manifold, namely ($S_l[\hat{x}_l(t)]$=0), it will be remained on the sliding manifold for later.*

Proof of Theorem 1. The Lyapunov function [44] is set below

$$\bar{V}(t) = \sum_{l=1}^{N} \frac{1}{2} S_l^2[\hat{x}_l(t)] \quad (26)$$

So, taking the derivative of $\bar{V}(t)$ and combine with Equation (23), we have:

$$\begin{aligned}\dot{\bar{V}}(t) = \sum_{l=1}^{N} \Big\{ &S_l^T[\hat{x}_l(t)] \times \left[\varepsilon_{l3} G_l \mathcal{A}_l \hat{x}_i(t) + \varepsilon_{l2} G_l B_l K_l \hat{x}_l(t)\right. \\ &+ \varepsilon_{l1} G_i L_i[\dot{y}_l(t) - \dot{\hat{y}}_l(t)] + Z_l \dot{\sigma}_l[\hat{x}_l(t)] \\ &\left. + \varepsilon_{l1} G_l C_{lk} \dot{\hat{x}}_k(t) + \varepsilon_{l1} G_l B_l \dot{u}_l(t)\right] \Big\} \quad (27)\end{aligned}$$

Using the control law ($u_l{}^{HO}(t)$) in Equation (24), Equation (27) becomes

$$\dot{\bar{V}}(t) = -\sum_{l=1}^{N} \delta_l S_l^2[\hat{x}_l(t)] \quad (28)$$

From Equation (28), clearly, $\dot{\tilde{V}}(t)$ is less than zero, which presents that the reachability of the system trajectory based on estimated SSVs of state observer in the MAPS with proposed controller in Equation (14) towards the sliding manifold and remain thereafter. □

3.4 | Stability analysis of the whole system

The stability of the whole system is proven in this section. The suggested method concentrates on the ultimate boundary of the signals. The entire system can converge to a steady state if only the state observer is to converge, and the SMC rule is capable of driving the system trajectory to the sliding surface in finite time. Then substituting $u_l^{eq}(t)$ in Equation (21) into the MAPS in Equation (14), we achieve

$$\begin{aligned}\dot{x}_l(t) &= [(1-\varepsilon_{l3})\mathcal{A}_l - \varepsilon_{l4}B_lK_l]x_l(t) + \omega_l(t) + \Omega_l\tilde{x}_l(t)\\ &\quad + [I_l - B_l(G_lB_l)^{-1}G_l]C_{lk}\tilde{x}_k\end{aligned} \tag{29}$$

where $\tilde{x}_l(t) = x_l(t) - \hat{x}_l(t)$ is the difference of the estimated and real states. $\varepsilon_{l3} = \dfrac{(\varepsilon_{l1}-\varepsilon_{l2})}{\varepsilon_{l1}}$; $\varepsilon_{l4} = \dfrac{\varepsilon_{l2}}{\varepsilon_{l1}}$; and $\Omega_l = (\varepsilon_{l3}\mathcal{A}_l + \varepsilon_{l4}B_lK_l) - B_l(G_lB_l)^{-1}G_lL_lF_l$

Assumption 3. the disturbance is $\omega_l(t)$ and the differential of $\omega_l(t)$ is bounded. There is an existence of the known scalars γ_l and $\bar{\gamma}_l$ so that $\|\omega_l(t)\| \le \gamma_l$ and $\|\dot{\omega}_l(t)\| \le \bar{\gamma}_l$, where $\|.\|$ is matrix norm. Then the time derivative of $\tilde{x}_l(t)$ is described as follows

$$\dot{\tilde{x}}_l(t) = (\mathcal{A}_l - L_lF_l)\tilde{x}_l(t) + C_{lk}\tilde{x}_k(t) + \omega_l(t) \tag{30}$$

Theorem 2. *The sliding motion in Equation (19) is asymptotically stable if only there exists a symmetric positive definite matrix P_l, R_l, and positive scalars ϖ_l,μ_l, θ_l, ξ_l, and ρ_l ($l = 1, 2, 3,\ldots N$). Then following LMI below*

$$\begin{bmatrix}\Sigma_{l1} & 0 & \Omega_l^T & \Sigma_{l3}^T & \mathrm{P}_l^T & 0 & 0 & 0\\ 0 & \Sigma_{l1} & 0 & 0 & 0 & \mathrm{P}_l^T & \mathrm{C}_{kl}^T & \mathrm{R}_l^T\\ \Omega_l & 0 & -\varpi_l & 0 & 0 & 0 & 0 & 0\\ \Sigma_{l3} & 0 & 0 & -\mu_l & 0 & 0 & 0 & 0\\ \mathrm{P}_l & 0 & 0 & 0 & -\theta_l & 0 & 0 & 0\\ 0 & \mathrm{P}_l & 0 & 0 & 0 & -\varpi_l^{-1} & 0 & 0\\ 0 & \mathrm{C}_{kl} & 0 & 0 & 0 & 0 & -\xi_l & 0\\ 0 & \mathrm{R}_l & 0 & 0 & 0 & 0 & 0 & -\rho_l\end{bmatrix} < 0 \tag{31}$$

where

$$\begin{aligned}\Sigma_{l1} &= [(1-\varepsilon_{l3})\mathcal{A}_l - \varepsilon_{l4}B_lK_l]P_l\\ &\quad + P_l^T[(1-\varepsilon_{l3})\mathcal{A}_l - \varepsilon_{l4}B_lK_l]^T\end{aligned} \tag{32}$$

$$\Sigma_{l2} = (\mathcal{A}_l - L_lF_l)R_l + R_l^T(\mathcal{A}_l - L_lF_l)^T \tag{33}$$

$$\Sigma_{l3} = [I_l - B_l(G_lB_l)^{-1}G_l]P_l \tag{34}$$

Proof of Theorem 2. To demonstrate the stability of the sliding motion in Equation (19), we choose the Lyapunov function [44] as below

$$V(t) = \sum_{l=1}^{N}[x_l^T(t)P_lx_l(t) + \tilde{x}_l^T(t)R_l\tilde{x}_l(t)] \tag{35}$$

where $P_l, R_l > 0$ satisfied Equation (35). Then, taking the derivative of $V(t)$ and using Equations (29) and (30), and applying Lemma 1 we have

$$\begin{aligned}\dot{V}(t) = \sum_{l=1}^{n}\Big\{ & x_l(t)\big\{[(1-\varepsilon_{l3})\mathcal{A}_l - \varepsilon_{l4}B_lK_l]P_l\\ & + P_l^T[(1-\varepsilon_{l3})\mathcal{A}_l - \varepsilon_{l4}B_lK_l]^T + \varpi_l\Omega_l\Omega_l^T\big\}x_l^T(t)\\ & + \tilde{x}_l(t)[(\mathcal{A}_l - L_lF_l)R_l + R_l^T(\mathcal{A}_l - L_lF_l)^T\\ & + \varpi_l^{-1}P_lP_l^T]\tilde{x}_l^T(t) + \mu_l^{-1}\tilde{x}_k(t)C_{lk}C_{lk}^T\tilde{x}_l^T(t)\\ & + \mu_lx_l(t)\Sigma_{l3}{\Sigma_{l3}}^Tx_l^T(t) + \nu_l\tilde{x}_k(t)C_{lk}C_{lk}^T\tilde{x}_k^T(t)\\ & + \nu_l^{-1}\tilde{x}_l(t)R_lR_l^T\tilde{x}_l^T(t) + \theta_lx_l(t)P_lP_l^Tx_l^T(t)\\ & + \theta_l^{-1}\omega_l(t)\omega_l^T(t) + \upsilon_l\tilde{x}_l(t)T_lR_l^T\tilde{x}_l^T(t)\\ & + \upsilon_l^{-1}\omega_l(t)\omega_l^T(t)\Big\}\end{aligned} \tag{36}$$

where ϖ_l, υ_l, ν_l are positive scalars. Since $\tilde{x}_k(t)C_{lk}C_{lk}^T\tilde{x}_k^T(t) = \tilde{x}_l(t)C_{kl}C_{kl}^T\tilde{x}_l^T(t)$ so Equation (36) becomes

$$\dot{V}(t) < \sum_{l=1}^{N}x_l(t)\Theta_{l1}x_l^T(t) + \tilde{x}_l(t)\Theta_{l2}\tilde{x}_l^T(t) + \kappa_l^{-1}\omega_l(t)\omega_l^T(t) \tag{37}$$

where

$$\begin{aligned}\Theta_1 &= [(1-\varepsilon_{l3})\mathcal{A}_l - \varepsilon_{l4}B_lK_l]P_l\\ &\quad + P_l^T[(1-\varepsilon_{l4})\mathcal{A}_l - \varepsilon_{l4}B_lK_l]^T\\ &\quad + \varpi_l\Omega_l\Omega_l^T + \mu_l\Sigma_{l3}\Sigma_{l3}^T + \theta PP_l^T;\end{aligned} \tag{38}$$

$$\begin{aligned}\Theta_2 &= (\mathcal{A}_l - L_lF_l)R_l + R_l^T(\mathcal{A}_l - L_lF_l)^T\\ &\quad + \varpi_l^{-1}P_lP_l^T + \zeta_lC_{kl}C_{kl}^T + \sigma_lR_lR_l^T;\end{aligned} \tag{39}$$

and $\kappa_l^{-1} = \theta_l^{-1} + \upsilon_l^{-1}; \zeta_l = \mu_l^{-1} + \nu_l; \sigma_l = \nu_l^{-1} + \upsilon_l$.

Define the augmented vector

$$\chi_l(t) = \begin{bmatrix}x_l(t) & \tilde{x}_l(t)\end{bmatrix}^T \tag{40}$$

In addition, by employing Lemma 2, LMI is equivalent to this inequality

$$\begin{bmatrix}\Theta_{l1} & 0\\ 0 & \Theta_{l2}\end{bmatrix} = -\mathrm{Y}_l < 0 \tag{41}$$

According to Equations (40) and (41), we obtain

$$\dot{V}(t) \leq \{-\lambda_{\min}[(\Upsilon_l)||\chi_l(t)||^2] + \iota_l\} \tag{42}$$

where the constant value $\iota_l = \kappa_l^{-1}\gamma_l^2$ and the eigenvalues of $\lambda_{\min}(\Upsilon_l) > 0$.

Therefore, $\dot{V}(t) < 0$ is achieved with $||\chi_l(t)|| > \sqrt{\frac{\iota_l}{\lambda_{\min}(\Upsilon_l)}}$. Hence, the sliding motion of MAPS in Equation (19) is asymptotically stable. □

4 | THE APPLIED HONEY BADGER ALGORITHM

HBA [29] is a novel nature-inspired meta-heuristic algorithm, which means, it was built based on mimicking the hunting behaviour of the honey badger species. HBA was proposed recently and its performance is superior to other state-of-the-art meta-heuristic algorithms proposed before such as simulated annealing (SA), PSO, covariance matrix adaptation with evolution strategies (CMA-ES), a success-history based parameter adaptation for differential evolution with linear population size reduction strategy (L-SHADE), moth-flame optimization (MFO), whale optimization algorithm (WOA), grasshopper optimisation algorithm (GOA), thermal exchange optimization (TEO), and HHO while tested by CEC'17 serial benchmark functions and four engineering design problems in practice.

The main difference between HBA and other meta-heuristic algorithms in the same class is the update process for new solutions. The presence of a reference index (RI) in the HBA update mechanism has reduced the probability of trapping into the local optima of the whole optimization process. The consideration of handling the local optima is highly focused while developing HBA. The process is conducted by selecting one out of two separate methods: the ditch creating method and the honey flavour guided method. These stages will be described in detail in the sub-sections below. Before the update process is carried out, there are several terms that must be calculated as follow:

$$\mathrm{IL} = rd_2 \times \frac{\mathrm{OS}}{4\pi l^2} \tag{43}$$

where

$$\mathrm{OS} = (S_n - S_{n+1})^2 \tag{44}$$

and

$$l = S_{pp} - S_n \tag{45}$$

where IL is the intensity level caused by the prey; OS is the original concentration source; rd_2 is the random value generated in the interval of [0,1]; l is the distance from the honey badger to the prospect prey; S_n is nth solution of the population ($n = 1, 2, .., Np$); S_{pp} is prey position. Next, the density indicator is proposed to support the whole searching process of HBA becoming more efficient. The determination of the density indicator is presented below

$$\varepsilon = \mathrm{CV} \times \exp\left(\frac{-\mathrm{It}}{\mathrm{It}^{\max}}\right) \tag{46}$$

where CV is a constant value. Normally, CV is greater than one and its value used in HBA is set by 2, It is the current iteration, and $\mathrm{It}^{\max}$ is the maximum quantity of iteration.

4.1 | The ditch creating method

The main purpose of this stage is to support the honey badger to determine approximately the position of the prospective prey in a specific area by using its smelling ability. Note that, the honey badger's position is continuously changed to get closer to the prey. This behaviour is expressed by the mathematical equation below

$$S_n^{\mathrm{new}} = S_{pp} + \mathrm{RI} \times \mathrm{DF} \times \mathrm{IL}_i \times S_{pp} + \mathrm{RI} \times rd_3 \times \varepsilon \times l_i |\cos(2\pi \times rd_4) \times [1 - \cos(2\pi \times rd_5)]| \tag{47}$$

and

$$\mathrm{RI} = \begin{cases} 1 & \text{if } rd_6 \leq 0.5 \\ -1 & \text{others} \end{cases} \tag{48}$$

where RI is the reference index, this term will support the optimization process escape from the local optima, DF is the degree of gaining food while honey badger engages the hunting process.

By experiments, the value of DF is greater than 1 and DF is set by 6 in HBA; rd_3, rd_4, rd_5, and rd_6 are respectively the random values generated in the interval between 0 and 1.

4.2 | The honey flavour guided method

According to the nature of the honey badger, one of the most perennial foods of honey badger is honey. However, finding honey and getting honey from the beehive is not easy. Therefore, to increase the probability of success while searching for honey in a large area, the honey badger will collaborate with a navigator called a honey guide bird. This kind of bird will bring the honey badger to the point where the beehive is located. This collaboration is described by Equation (49) below

$$S_n^{\mathrm{new}} = S_{pp} + \mathrm{RI} \times rd_7 \times \varepsilon \times l \tag{49}$$

where rd_7 is a random value generated in the interval between 0 and 1.

The utilization of the ditch creating method or honey flavour guided method for the update process of HBA is dependent on the selection term (Str) which is the random value in the interval between 0 and 1. If Str is less than 0.5, the ditch creating method will be carried out. Otherwise, the honey flavour-guided method is selected.

Figure 2 depicts the flowchart of the entire searching process of the HBA. From which, the entire optimization process of

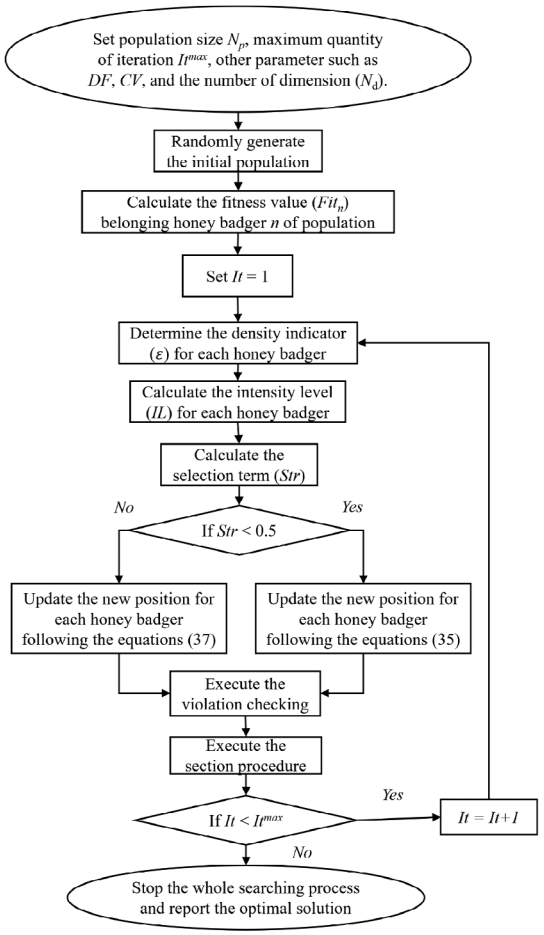

FIGURE 2 The entire searching process of HBA for the considered problem.

HBA that is utilized to get the optimal control parameters can be summarized in steps as below:

- Step 1: Set the control parameters, including the quantity of population (N_p), maximum quantity of iterations (It^{max}), the degree of gaining food (DF), the constant value (CV), and the number of dimensions (N_d). It is important to note that the value of (N_d) must be equal to the number of desired variables that need to be found for the problem under consideration. In this research, (N_d) is set to four, and the specific variables will be revealed in the next section. This also implies that there are four variables that must be determined to maximize the raw performance of the proposed controller, as mentioned in Section 3.
- Step 2: Randomly generate the initial population following the equation below:

$$S_n = \mathrm{LB}_n + \mathrm{RND} \times (\mathrm{UB}_n - \mathrm{LB}_n) \tag{50}$$

where S_n is the honey badger n with $n = 1,\ldots, N_p$. In the optimal process each S_n is considered a feasible solution of the considered problem which contains the set of desired variables as mentioned in Step 1. LB_n and UB_n are the lowest and highest boundaries of the solution S_n, respectively. The boundaries also contain the lowest and the highest limits of the desired variables. That also means that, all the solutions of the initial population are only generated within their boundaries, and RND is the random value between 0 and 1.

- Step 3: Calculate the fitness value (Fit_n) belonging honey badger n of population. The mathematical expression of the fitness function will be reveal in the next section.
- Step 4: Set the initial iteration at 1 (It = 1).
- Step 5: Determine the density indicator (ε) for each honey badger using Equation (46).
- Step 6: Calculate the intensity level (IL) for each honey badger using Equation (43).
- Step 7: Randomly generate Str then, update new position for honey badger n using Equation (45) if Str < 0.5, otherwise using Equation (49).
- Step 8: Execute the violation checking. This step aims to make sure that, all the desired variables of the solution n locates inside the legal limits.
- Step 9: Execute the selection procedure. The main target in this step is to remain in the better position (better solution) for the next iteration and abandon the worse one.
- Step 10: Check the terminal condition. That means if the current number of iterations (It) is still less than the maximum quantity of iteration ($\mathrm{It}^{\max}$), increase the It by one and return to Step 5. Otherwise, terminate the whole computing process and report the optimization results.

5 | THE IMPLEMENTATION OF THE APPLIED ALGORITHMS FOR THE dHoSMO CONTROLLER DESIGN PROBLEM

In this section, three meta-heuristic methods are applied to determine the optimal control parameters for the dHoSMO controller. The first method used is PSO [55], the second method is TSO [56], and the last one is HBA [29]. These methods are nature-inspired algorithms that are developed based on the living practices of different species on the Earth. The only thing that differentiates the three applied methods is their update mechanisms for new solutions. Particularly, PSO utilizes the variations of both position and velocity belonged to each particle to produce the new solutions after each iteration. TSO employed the cooperative mechanism among the tunas in their foraging process to generate the new solutions. Lastly, HBA updates its new solution based on the execution of one out of two guide methods as mentioned in the previous section.

On the other hand, the main objective of this study is to apply the three methods mentioned earlier to determine the optimal solution to the considered problem and also indicate the best applied method among the three to deal with such a problem. Besides reaching the best solutions to the given problem, other targets of the whole paper are briefly summarized as follows:

1. Propose a new approach to determine the optimal control parameters of the controllers without using any complex

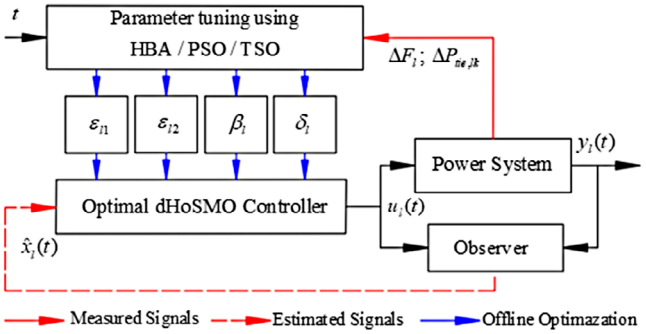

FIGURE 3 The block diagram of the HBA/PSO/TSO-based dHoSMO controller.

mathematical models as in previous studies. Particularly, this study applies PSO, TSO, and HBA to optimize all the important control parameters required by the PID and the newly proposed controller, which is dHoSMC.

2. The application of HBA is aimed at demonstrating the high capability of finding the optimal solution while compared to others, such as PSO and TSO, concerning execution time, the quality of the identified optimal solution, and computer resource requirements. This implies that the most effective method among the three will offer the best optimal control parameters for promptly addressing disturbances in the PS. This becomes crucial when there is an urgent requirement for a new set of control parameters to adapt to the evolving system status while ensuring that other relevant criteria remain within their defined limits.

The graphical illustration of executing the three algorithms to provide the control parameters for the controller is illustrated in Figure 3. In which, PSO, TSO and HBA determine the optimal parameters of the dHoSMO controller. Notably, the crucial parameters are ε_{i1}, ε_{i2}, β_i, and α_i.

The real performance of meta-heuristic methods is evaluated for the purpose of shortening the overshoot accompany with settling time. In order to reach that goal, the minimizing of the integral time absolute error (ITAE) objective function is utilized to be the main objective function. Moreover, the effectiveness of PSO, TSO, and HBA is clarified whilst these methods are tested by the main objective function in two separate cases including SAPS and MAPS. The mathematical expressions belonging to ITAE objective function in two cases can be presented respectively in Equations (51) and (52) below.

$$\mathrm{ITAE}_{\mathrm{SAPS}} = \int_0^{t_{\mathrm{sim}}} |\Delta F_i| t \mathrm{d}t \tag{51}$$

and

$$\mathrm{ITAE}_{\mathrm{MAPS}} = \int_0^{t_{\mathrm{sim}}} \left(\sum_{i=1}^{N} |\Delta F_i| + \sum_{i=1;k\neq i}^{M} |\Delta P_{\mathrm{tie},ik}| \right) t \mathrm{d}t \tag{52}$$

where t and t_{sim} are simulation time and total simulation time, respectively. It should be noted that ITAE defined in Equations (51) and (52) serves as the simple objective function due to its benefits in minimizing both undershoot/overshoot and settling time, as employed in [52, 54], for both SAPS and MAPS.

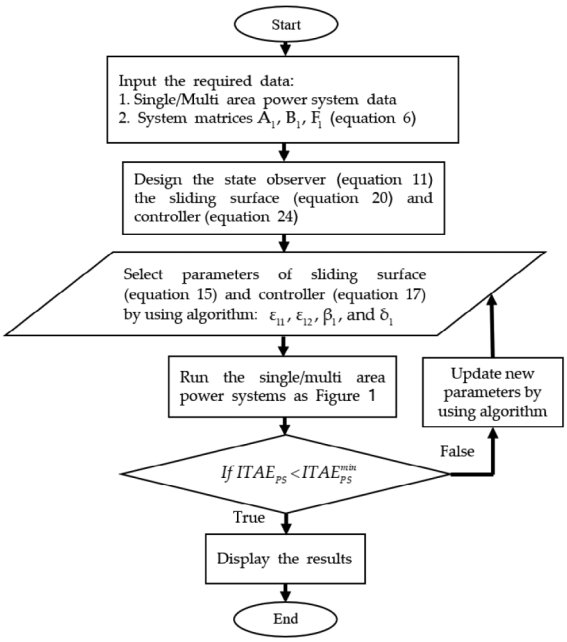

FIGURE 4 The flowchart of the optimal frequency control scheme.

6 | SIMULATION RESULTS AND ANALYSIS

In this section, the simulations of case studies are performed to examine the effectiveness of the suggested control scheme as shown in Figure 4. Both SAPS and MAPS are utilized for the simulation case studies. To present the superior performance of the proposed scheme, the result comparison is conducted based on maximum decreased frequency fluctuations with PSO-PID, TSO-PID, HBA-PID, PSO-dHoSMO, TSO-dHoSMO, HBA-dHoSMO, and the study [50]. IEEE 39-bus New England test system is employed and compared with study [43] to assess the reliability and robustness as well as its highly applicable of the proposed controller in large-scale PS.

6.1 | Determination of the control parameters of the applied algorithms

The control parameters of HBA in terms of population size (N_p) and maximum number of iterations ($\mathrm{IT}_{\mathrm{max}}$) are highly dependent on the complexity of the problems considered and the experience of the developer. However, the application of PSO, TSO, and HBA is intended to show the cutting-edge characteristics of a modern meta-heuristic algorithm, HBA, compared to the others, including PSO and TSO, while they are simultaneously applied to deal with the same optimization problem. Through the data presented in this study, the conclusion is that HBA is far more effective than PSO and TSO by

TABLE 1 Optimal controller parameters for SAPS.

Method	Parameters	PSO	HBA
	K_{P1}	6.18	20.23
PID	K_{I1}	50.00	50.00
	K_{D1}	0	8.63
	ε_{11}	2.63	0.14
dHoSMO	ε_{12}	49.90	49.90
	β_1	43.13	0.14
	α_1	0.10	0.14

TABLE 2 Optimal controller parameters for two-area PS.

Method	Parameters	PSO ($l = 1/2$)	HBA ($l = 1/2$)
	ε_{l1}	0.10/0.10	0.10/0.10
dHoSMO	ε_{l2}	2.34/49.90	1.01/27.27
	β_l	2.69/0.10	4.08/4.86
	α_l	0.10/49.90	4.01/4.98

offering a better optimal value of fitness function while using the same initial control parameters. If both N_p and $\mathrm{IT}_{\max}$ are set at very high values as shown while dealing with the benchmark functions shown in [29], an optimal solution may be found by the three, but the computing time will be longer, and the effectiveness of the applied algorithms cannot be judged clearly.

As mentioned earlier, this study tries to solve a practical problem in power system operation, therefore, an algorithm with long computing time is not a proper selection. The experiments to select the optimal control parameters were conducted with different values of both N_p and $\mathrm{IT}_{\max}$. The results obtained by these experiments led to the decisions of N_p and $\mathrm{IT}_{\max}$ as shown in this study which are 50 and 100, respectively.

The implementation of the three applied algorithms to deal with the given problem will be executed as follows: Firstly, HBA and PSO will be applied to determine the optimal control parameters for the proposed controller in the SAPS. Then, both HBA and PSO will be implemented in the MAPS for evaluating their real performance. Besides, TSO will join the evaluation in this case along with HBA and PSO. As mentioned earlier, TSO is proposed earlier than HBA by one year, and the implementation of TSO in this case is aimed at giving more evidence while judging the real efficiency of HBA, especially when the scale of the given problem is substantially larger.

6.2 | LFC with step load disturbances

The parameters of the PID and dHoSMO controllers are first optimized by PSO and HBA. Based on the findings in the literature and design experience, the boundary of the controller parameters is in a range of [0, 50], following the work in refs. [50, 53]. After that, these parameters are utilized by the controller to minimize the main objective function. The results of SAPS and MAPS are fully shown in Tables 1 and 2, respectively.

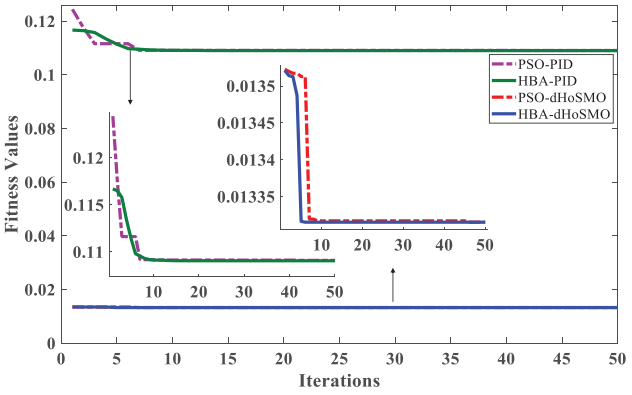

FIGURE 5 The best fitness values of HBA and PSO combined with PID and dHoSMO for SAPS.

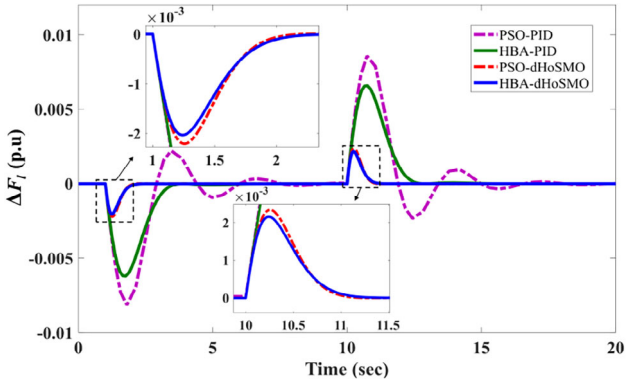

FIGURE 6 Frequency fluctuations of HBA and PSO combined with PID and dHoSMO for SAPS.

6.2.1 | Single-area power system

A SAPS model with the widely used parameters of the governor, non-reheated turbine, and generator is employed to evaluate the effectiveness of the proposed LFC scheme in this case. The parameters of SAPS [50] are listed as follows: $K_{P1} = 1$, $T_{P1} = 10$, $T_{M1} = 0.3$, $T_{V1} = 0.1$, $K_{I1} = 50$, $\beta_1 = 0.4$, and $R_1 = 0.055$. Two times of changed load disturbances are employed to the system with +0.16 [pu] at 1 [s] and −0.17 [pu] at 10 [s]. Figure 5 shows the best convergence curves obtained by four different control approaches, namely the PSO-PID, the HBA-PID, the PSO-dHoSMO,the HBA-dHoSMO, respectively. From which the *y*-axis is the fitness values and the *x*-axis is the number of iterations. As shown in Figure 6, it is easy to observe that the proposed controller decreases the peak-value of frequency deviation (ΔF_l) as well as makes less amount of finite time in comparison with other approaches. The efficiency of LFC in eliminating load disturbances is able to be enhanced when applying the suggested controller. The superiority performance of the HBA is also clearly expressed via both PID and dHoSMO controllers in comparison with PSO over settling time and overshoot. The values of frequency deviation overshoot for each scheme are presented in Table 3. As shown in Table 3, the four different control approaches outperform the PSO-SMC and ADP-SMC methods proposed by Mu et al. [50].

TABLE 3 The value of absolute ITAE function and frequency deviation in SAPS.

Method	PSO-PID	HBA-PID	PSO-dHoSMO	HBA-dHoSMO	PSO-SMC [50]	ADP-SMC [50]
$ITAE_{SAPS}$	0.1092	0.1091	0.0136	**0.0133**	0.0753	0.0733
$Max(\Delta F_1)$	8.57×10^{-3}	6.55×10^{-3}	2.34×10^{-3}	$\mathbf{2.15 \times 10^{-3}}$	3.29×10^{-3}	3.49×10^{-3}

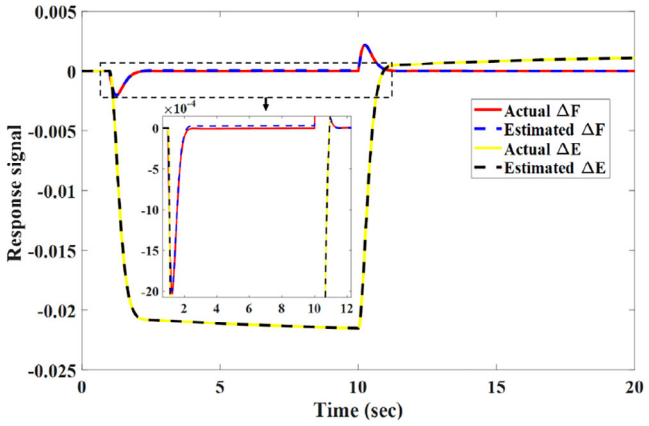

FIGURE 7 Actual and estimated response signals of the proposed method.

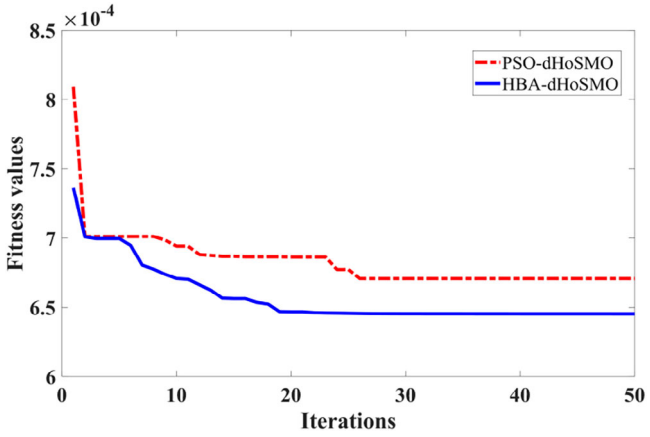

FIGURE 8 The best fitness values of PSO-dHoSMO and HBA-dHoSMO for two-area PS along the iteration.

Additionally, Table 3 also highlights the improvement of higher-order SMC compared to SMC. Based on the results, it can be concluded that the higher-order SMC approaches are superior to classical ones. Similarly, the HBA approach outperforms the PSO-based and ADP-based approaches.

As shown in Figure 7, the actual and estimated response signals of turbine power output and frequency deviation are almost identical. It implied that the designed state observer fast converges and provides a precise estimate only based on system input and output.

Remark 2. In this case, it is easy to observe from Figure 6. The frequency fluctuation given by the PID-based controller is not good enough. Clearly, the PSO and HBA-based control provide the smallest absolute frequency fluctuation during the entire regulation. However, the dHoSMO controller based on PSO and HBA provides superior performance with smaller overshoots and faster settling times. Therefore, in the following case, we only carry out the dHoSMO controller with HBA and PSO to compare the algorithm performance.

6.2.2 | Two-area power system

The proposed LFC scheme is evaluated on a widely used two-area PS. The parameters of two-area PS [50] are listed as follows: $K_{P1} = 1$, $K_{P2} = 6.67$, $T_{P1} = 10$, $T_{P1} = 8$, $T_{M1} = 0.3$, $T_{M2} = 0.4$, $T_{V1} = 0.1$, $T_{V1} = 0.17$, $K_{I1} = K_{I2} = 0.1$, $\beta_1 = \beta_2 = 0.4$, and $R_1 = R_2 = 0.055$. A disturbance load is executed in area 1 with values as +0.1 [pu] at 1s. Subsequently, these parameters are updated to Equations (1)–(13) as well as the dynamics equations in Figure 1.

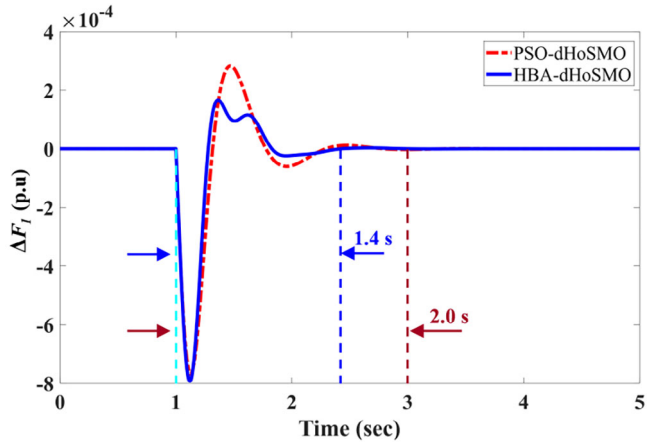

FIGURE 9 Frequency fluctuations in Area 1 of two-area PS using PSO-dHoSMO and HBA-dHoSMO.

The best fitness values (y-axis) obtained by two algorithms, namely PSO and HBA, with dHoSMO are presented along the number of iterations (x-axis) as shown in Figure 8. Clearly, the HBA technique demonstrates outstanding performance with fast convergence at the 20th iteration and lower best fitness at 6.5×10^{-4}, compared with the 26th iteration and 6.75×10^{-4} of PSO. The corresponding results of frequency fluctuations in areas 1 and 2 are respectively illustrated in Figures 9 and 10. In Figure 9, the settling time of the HBA-dHoSMO is lower than the PSO-dHoSMO, indicating that the HBA-dHoSMO is better than the PSO-dHoSMO in area 1. Similarly, HBA-dHoSMO is

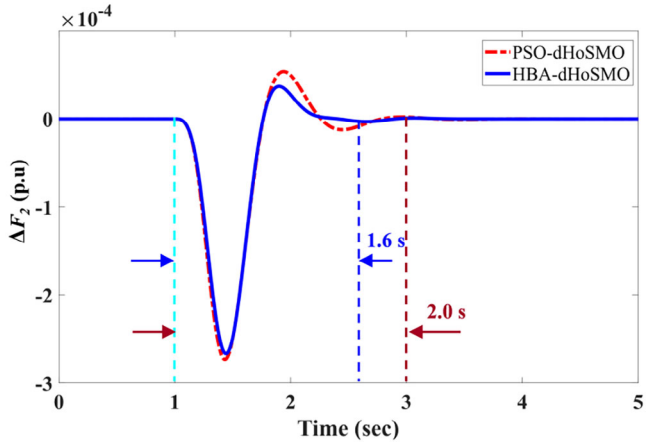

FIGURE 10 Frequency fluctuations in Area 2 of two-area PS using PSO-dHoSMO and HBA-dHoSMO.

TABLE 4 The value of response signals in two-area PS.

Method	PSO-dHOSMO	HBA-dHOSMO
$ITAE_{MAPS}$	6.71×10^{-4}	6.45×10^{-4}
$Max(\lvert\Delta F_1\rvert)$	7.91×10^{-4}	7.92×10^{-4}
$Max(\lvert\Delta F_2\rvert)$	2.72×10^{-4}	2.66×10^{-4}
$Max(\lvert\Delta P_{tie,12}\rvert)$	4.95×10^{-4}	4.59×10^{-4}

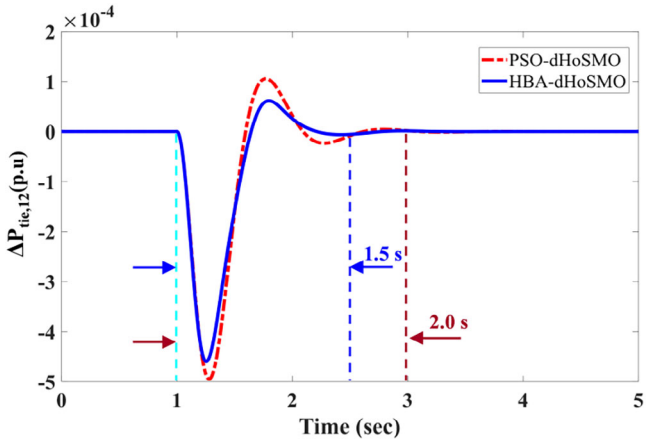

FIGURE 11 Tie-line power fluctuations of two-area PS using PSO-dHoSMO and HBA-dHoSMO.

also better than PSO-dHoSMO in area 2, as shown in Figure 10. The performance analysis of the suggested scheme is displayed in Table 4. It is asserted that the suggested scheme has much-enhanced system performance compared to another one in terms of settling time and under/overshoot. Lastly, Figure 11 depicts tie-line power between the first and second areas, compared to PSO-dHoSMO, the value of tie-line power fluctuation applied HBA for dHoSMO controller is lower overshoot and smaller time of convergence.

In particular, the simulation result reports indicate an effect of the proposed controller with HBA in comparison with

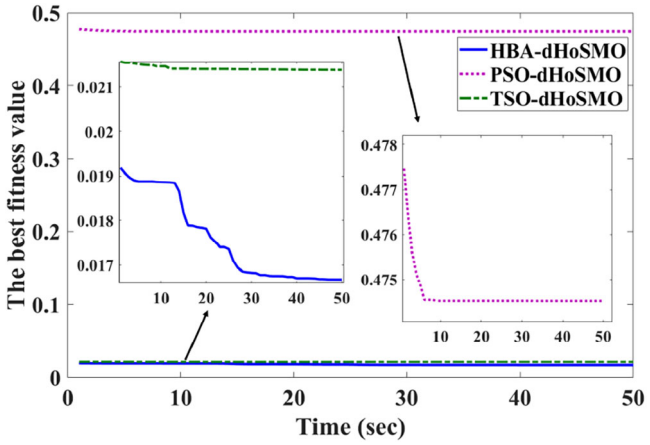

FIGURE 12 Best fitness values of PSO-dHoSMO, TSO-dHoSMO, and HBA-dHoSMO for three-area PS along the iteration.

TABLE 5 Frequency and time-line power deviations of three-area PS.

	HBA		TSO		PSO	
Methods	Max.O.S (pu)	Ts (s)	Max.O.S (pu)	Ts (s)	Max.O.S (pu)	Ts (s)
ΔF_1	−0.0168	0.51	−0.0322	0.87	−0.0250	0.85
ΔF_2	−0.0356	0.60	−0.0356	0.51	−0.0277	1.08
ΔF_3	−0.0291	0.54	−0.0440	0.90	−0.0243	1.11
ΔP_{tie12}	−0.0089	0.37	−0.0139	0.55	−0.0108	1.00
ΔP_{tie23}	−0.0031	0.70	0.0020	1.38	0.0023	0.74
ΔP_{tie31}	0.0055	0.47	−0.0028	1.13	0.0011	0.86

PSO. Clearly, the controller with HBA is well-designed for bringing frequency deviation to zero fastest as well as the smallest overshoot.

6.2.3 | Three-area power system

In this scenario, we evaluate the proposed controller (dHoSMO) in a three-area PS under communication delays to compare the effectiveness of HBA with TSO and PSO. The PS parameters are consistent with those used in a prior study [36]. The load disturbances in the three areas are respectively set at 0.1[pu], 0.15[pu], and 0.15[pu] at 1s for the first, second, and third areas. The optimal fitness values of the three methods are presented in Figure 12, indicating that HBA performs better than TSO and significantly outperforms PSO. Specifically, the ITAE values are 0.0167 for HBA, 0.0214 for TSO, and 0.4745 for PSO. Additionally, the frequency and tie-line power deviation of the three-area PS with a time delay of 0.1 s are depicted in Figures 13 and 14, and detailed results are provided in Table 5. It is evident that HBA achieves superior results in terms of settling time and overshoot compared to other algorithms.

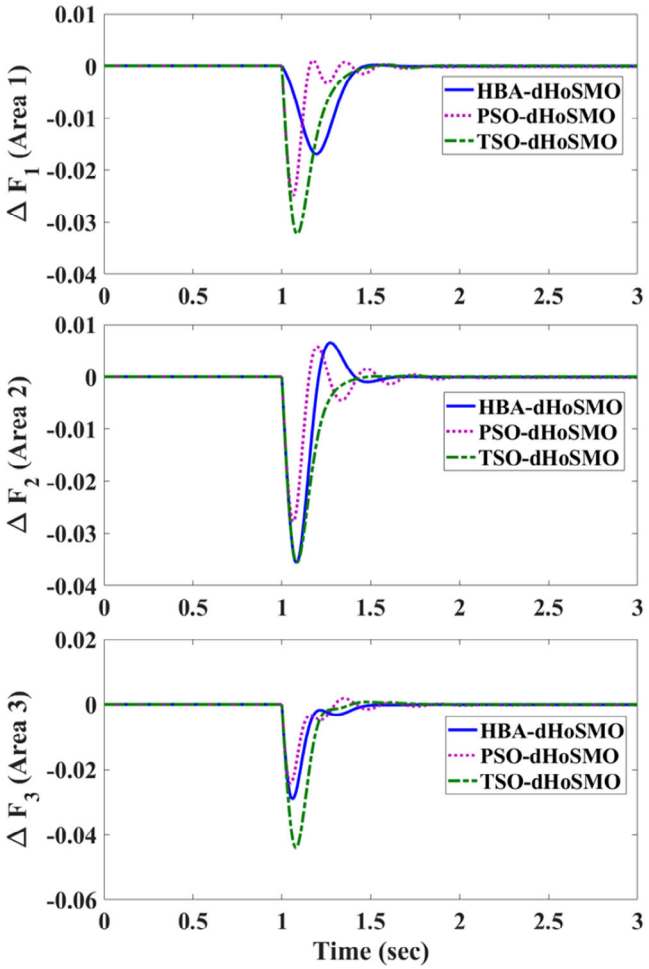

FIGURE 13 Frequency deviation of three-area PS under communication delay using PSO-dHoSMO, TSO-dHoSMO, and HBA-dHoSMO.

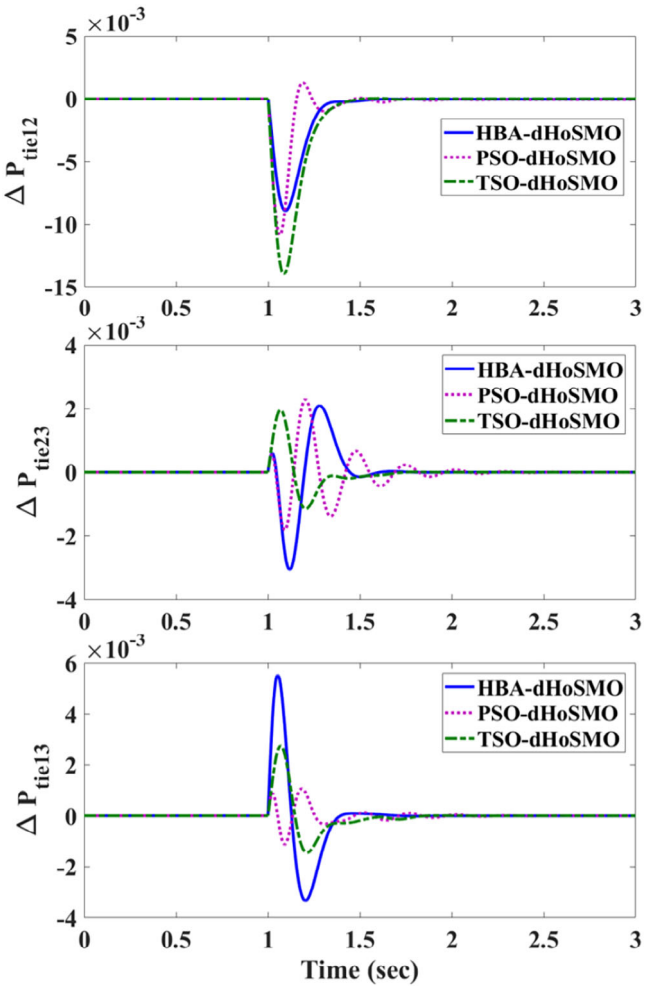

FIGURE 14 Tie-line power fluctuations of three-area PS under communication delay using PSO-dHoSMO, TSO-dHoSMO, and HBA-dHoSMO.

6.3 | MAPS with proposed approach against parameter uncertainties and step load disturbances

To evaluate the further effectiveness of the proposed scheme, the four worst scenarios are employed to demonstrate the controller robustness and reliability with some assumptions in various parameters of two-area PS. The nominal values of system parameters are selected to be the same as [50], where three parameters (T_{Pl}, T_{Vl}, and R_l) were assumed to change as Table 6. These parameters are subsequently updated to the matrix A_l in Equation (10), B_l in Equation (11), C_{lk} in Equation (12), D_l in Equation (13), and the dynamics equations in Figure 1. Consequently, altering these parameters introduces nonlinearities into the system. However, these changes must adhere to assumptions 1 and 2 to ensure the system dynamics remain stable even in the presence of minor nonlinear effects.

Figure 15 depicts the system response signals of a two-area PS with only the primary controller on the left and the proposed controller on the right. Figure 15(a) and Figure 15(b) show the frequency fluctuations without and with the pro-

TABLE 6 The parameter variations in two-area PS.

Parameter ($l = 1/2$)		Nominal values	Variation range [%]	Updated values
Case 1	T_{Pl}	10/8	+25	12.5/10
	T_{Vl}	0.1/0.17	−25	0.075/0.1275
	R_l	0.055/0.055	−25	0.04125/0.04125
Case 2	T_{Pl}	10/8	−25	7.5/6
	T_{Vl}	0.1/0.17	+25	0.125/0.2125
	R_l	0.055/0.055	+25	0.06785/0.06785
Case 3	T_{Pl}	10/8	+50	15/12
	T_{Vl}	0.1/0.17	−50	0.05/0.0855
	R_l	0.055/0.055	−50	0.0275/0.0275
Case 4	T_{Pl}	10/8	−50	5/4
	T_{Vl}	0.1/0.17	+50	0.15/0.255
	R_l	0.055/0.055	+50	0.0825/0.0825

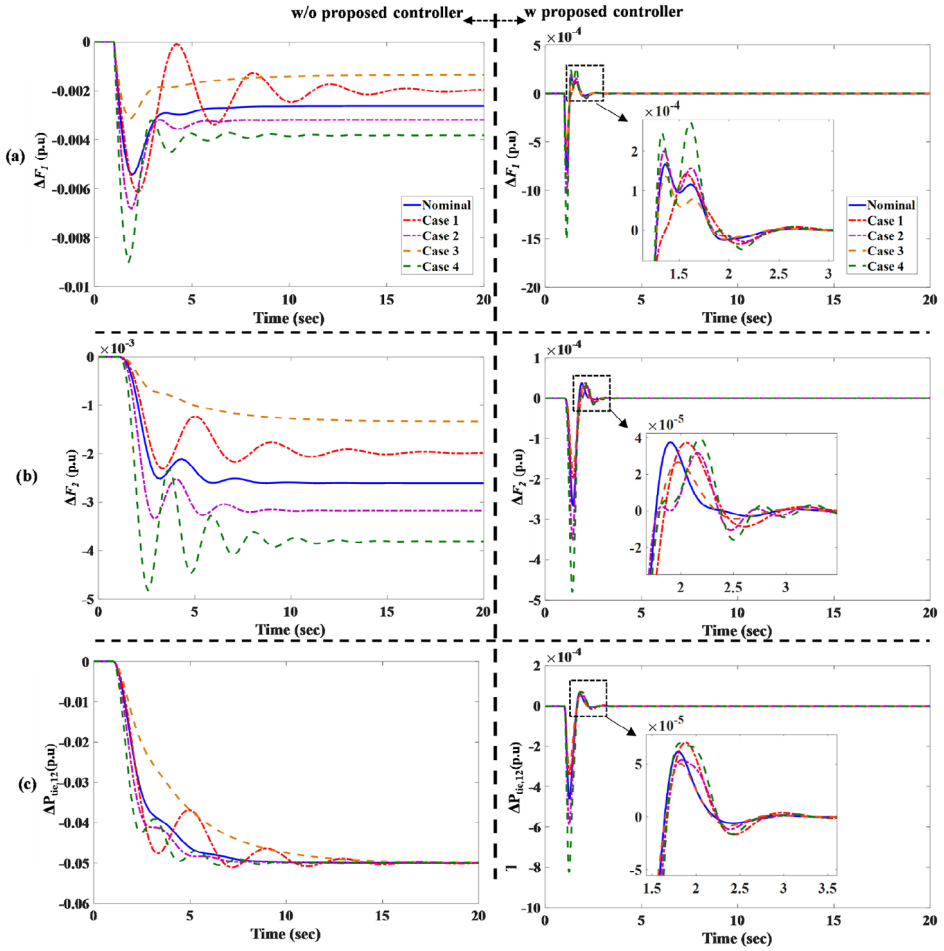

FIGURE 15 The system response signals of two-area PS with and without proposed control method under parameter uncertainties and step load disturbances: (a) frequency fluctuations in 1st area, (b) frequency fluctuations in 2nd area, and (c) tie-line power variation.

posed controller applied on areas 1 and 2, respectively. It can be observed that when the suggested controller is involved, the time length making frequency deviations return to zero is highest at approximately 3 [s], and the maximum overshoot is 15×10^{-4} [pu]. The tie-line power fluctuation is also represented in Figure 15(c). Clearly, the proposed scheme has given high stability while coping with plant uncertainties even though a wide range of deviations has been employed.

Remark 3. The testing results in this case indicated that the system is effective and robust under non-linear system with the same conditions as in [52].

6.4 | IEEE 39-bus New England PS

The performance of the designed controller is assessed again in this section via a large-scale real-test system. The IEEE-39 node configuration of New England PS is utilized to carry out the test for the controller performance. The system includes 10 generators and these are distributed in three separate governable zones. There are three generators located in each governable zones 1 and 2. The four remaining generators are all operated in governable zone 3. In addition, all generators in the whole system are simultaneously operated during normal operation. Finally, the single graph illustration of the IEEE-39 node configuration [43] is illustrated in Figure 16.

To conduct a fair comparison regarding the working performance of the proposed method, we have utilized the same testing condition with study [43] including load variations as shown Figure 18 and system parameters as shown in Table 7. In addition, the main goal of the entire research is to reduce as much as possible the maximum over/undershoot (Max.O.S) and the settling time (T_s). To reach that goal, a meta-heuristic algorithm called HBA is applied to deal with objective functions as mentioned earlier. As a result, the performance of the proposed method is improved whilst compared with study [43] shown Table 8.

Finally, the convergence curve given by HBA after 50 iterations is described in Figure 17. The frequency deviations and the tie-line power fluctuations for three areas are shown in Figures 19 and 20, respectively.

Remark 4. From simulation results, it is clear that the proposed approach is not only considered to be a highly effective one but also a reliable characteristic proved during the experience

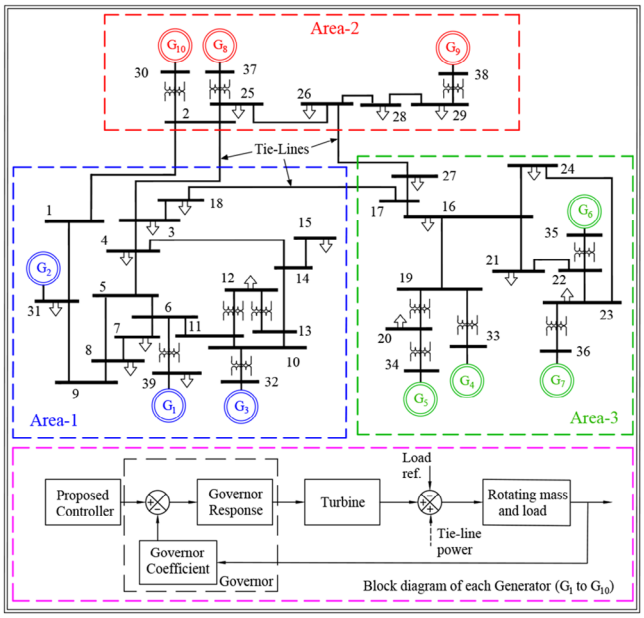

FIGURE 16 The structure of IEEE 39-bus New England PS.

TABLE 7 Parameters of IEEE 39-bus New England system.

Generators (bus)	M_I	D_I	T_{VI}	T_{MI}
G1 (39)	3.0	4.0	0.25	0.2
G2 (31)	2.5	4.0	0.25	0.2
G3 (32)	4.0	6.0	0.25	0.2
G4 (33)	2.0	3.5	0.25	0.2
G5 (34)	3.5	3.0	0.25	0.2
G6 (35)	3.0	7.5	0.25	0.2
G7 (36)	2.5	4.0	0.25	0.2
G8 (37)	2.0	6.5	0.25	0.2
G9 (38)	6.0	5.0	0.25	0.2
G10 (30)	4.0	5.0	0.25	0.2

TABLE 8 IEEE 39-bus New England system frequency deviations.

	Proposed method		Observer-non-linear SMC [43]	
Methods	Max.O.S (p.u.)	T_s (s)	Max.O.S (p.u.)	T_s (s)
Area 1	0.0301	2.5	0.0316	4
Area 2	−0.0233	2.5	−0.0258	4
Area 3	−0.0316	2.5	−0.0428	4

simulations under several disturbance conditions. Therefore, the proposed method can absolutely deal with LFC issues in the large-scale, practical, MAPS.

Remark 5. The proposed approach has already been examined under several load disturbances and parameter uncertainties in this section. The case study results point out that the proposed approach is not only robust and effective with higher-order sliding surface and HBA approach but also highly applicable with the state observer and decentralized approach.

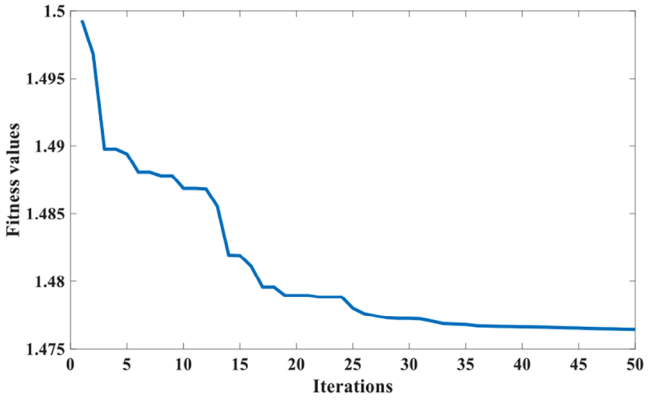

FIGURE 17 The best fitness of HBA-dHoSMO with New England PS.

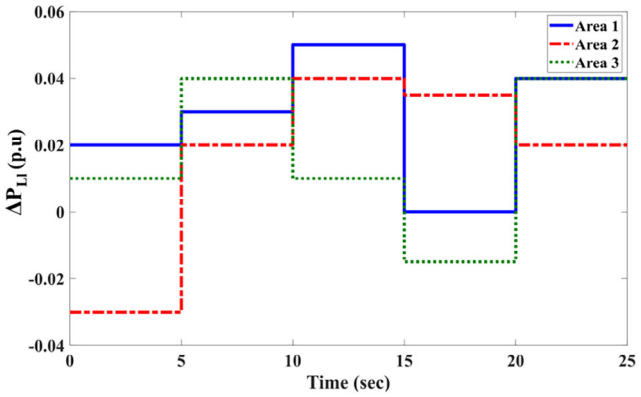

FIGURE 18 Load variations using HBA-dHoSMO for New England PS.

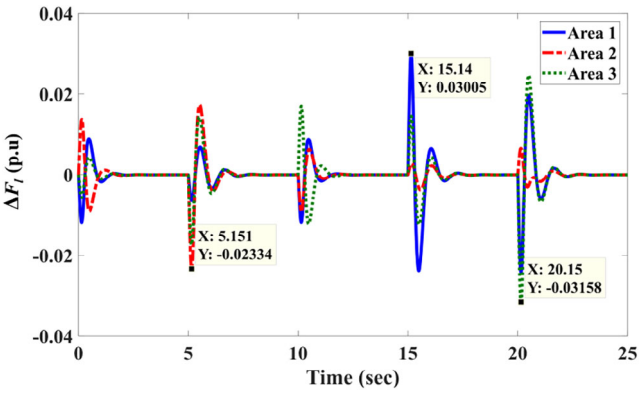

FIGURE 19 Frequency fluctuations using HBA-dHoSMO for New England PS.

6.5 | Discussion

In the single-area power system section, both PSO-based and HBA-based PID and SMC were simulated to demonstrate the

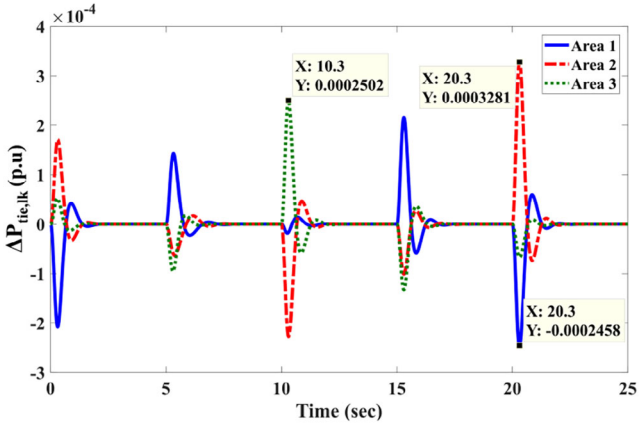

FIGURE 20 Tie-line power fluctuations using HBA-dHoSMO for New England PS.

effectiveness of the proposed algorithm and SMC. Then, PSO-based and ADP-based SMC were employed and compared with HBA under the same conditions in two-area PS section to emphasize again the robustness of HBA. Based on the obtained results, it was indicated that HBA is more effective than the previously published methods, such as PSO-based and ADP-based [50], thanks to the update mechanism for the new solution.

In addition, to assess the robustness of the proposed high-order SMC under a larger-scale system, continuous changes in the plant parameters and the IEEE 39-bus New England PS were also employed. Accordingly, the simulation results showed that the proposed controller is more stable and practical in comparison to the other methods based on decentralized and continuous control approaches, with the main purpose being to eliminate the chattering and oscillating phenomena.

While HBA-dHOSMC offers advantages in terms of control performance, it can be more challenging to implement in real-world systems due to complexity, and sensitivity to noise. Some disadvantages of this method can be mentioned as:

1. Sensitivity to system dynamics: Higher-order sliding modes may be more sensitive to variations in PS dynamics, such as system parameters or operating conditions. This sensitivity can affect the robustness and performance of the control system.
2. Computational resources: can be computationally intensive, which may pose challenges in real-time implementation in PS applications, especially in large-scale systems with multiple control loops.
3. Moreover, thanks to the evolution algorithm, complex requirements of careful tuning of control parameters have been effectively solved.

7 | CONCLUSION

In this study, a dHoSMO controller integrated HBA technique is designed for LFC in SAPS and MAPS. The state observer is used to estimate exactly local SSVs based on system input and output. Therefore, the suggested controller is quite simple for practical implementation. Then, the higher-order sliding surface is constructed to improve system performance by eliminating the chattering issue. During the controller designing process, the entire system stability has been theoretically demonstrated via Lyapunov stability theory with LMI. Regarding the suggested controller design, the HBA, TSO and PSO techniques were further developed, while the PID method is also considered to be compared method. Experimental simulations are carried out on single-, two-, and three-area PSs as well as three-area New England 39-bus testing systems. The results indicate that the proposed control scheme can significantly decrease frequency fluctuations and tie-line power deviations while compared with other control schemes under several load disturbances and parameter uncertainties. The proposed control scheme (HBA-dHoSMO) has obtained the ITAE values of 0.0133, 6.45×10^{-4}, and 0.0167 for single-, two, and three-area PSs. This indicates its effectiveness in both single- and multi-area PSs. In our future research, we intend to assess the robustness of our proposed approach within intricate power systems comprising diverse sources, including a substantial penetration of renewable energy sources. The incorporation of energy storage systems will enhance the LFC loop. Moreover, we plan to conduct practical validations using both laboratory setups and real-time digital simulators to validate the effectiveness, stability, and robustness of the proposed control scheme. In subsequent work, the integration of grid-forming inverters to enhance the further validation of our proposed control methods, as it represents a promising research direction in the field.

NOMENCLATURE

AGC	Automatic generation control
AI	Artificial intelligence
ASO	Atom search optimization
CMA-ES	Covariance matrix adaptation with evolution strategies
dHoSMO	Decentralized higher-order sliding mode observe
DSA	Dragonfly search algorithm
FOPID	Fractional order PID
GOA	Grasshopper optimisation algorithm
GSA	Gravitational search algorithm
HBA	Honey badger algorithm
HHO	Harris Hawk optimization
ITAE	Integral time absolute error
LFC	Load frequency control
LMI	Linear matrix inequality
L-SHADE	Success-history based parameter adaptation for differential & evolution with linear population size reduction strategy
MAPS	Multi-area power systems
PID	Proportional-integral-derivative
PS	Power system
PSO	Particle swarm optimization
RI	Reference index

RFB	Redox flow battery
SA	Simulated annealing
SAPS	Single-area power system
SMC	Sliding mode control
SSVs	System state variables
TEO	Thermal exchange optimization
WOA	Whale optimization algorithm

AUTHOR CONTRIBUTIONS

Anh-Tuan Tran: Conceptualization; methodology; software; validation; data curation; writing—original draft. **Minh Phuc Duong**: Methodology; software; validation; writing—original draft. **Nhat Truong Pham**: Methodology; software; validation; writing—review and editing. **Jae Woong Shim**: Methodology; project administration; writing—review and editing; supervision.

ACKNOWLEDGMENTS

This work was supported by the National Research Foundation of Korea (NRF) Grant by the Korean Government through MSIT under Grant 2021R1C1C1012806. This study was supported by the Basic Research and Development Project Research Fund of Korea Electric Power Corporation under Grant No. R21XO02-2.

CONFLICT OF INTEREST STATEMENT

The authors declare no conflicts of interest.

DATA AVAILABILITY STATEMENT

Data sharing is not applicable to this article as no new data were created or analyzed in this study.

ORCID

Nhat Truong Pham https://orcid.org/0000-0002-8086-6722
Jae Woong Shim https://orcid.org/0000-0001-5257-934X

REFERENCES

1. Grigsby, L.L.: Power System Stability and Control. CRC Press, Boca Raton, FL (2007)
2. Bevrani, H.: Robust Power System Frequency Control. Springer, Berlin, Heidelberg (2014)
3. Su, X., Liu, X., Song, Y.D.: Event-triggered sliding-mode control for multi-area power systems. IEEE Trans. Ind. Electron. 64(8), 6732–6741 (2017)
4. Mi, Y., Hao, X., Liu, Y., Fu, Y., Wang, C., Wang, P., et al.: Sliding mode load frequency control for multi-area time-delay power system with wind power integration. IET Gener. Transm. Distrib. 11(18), 4644–4653 (2017)
5. Onyeka, A.E., Xing-Gang, Y., Mao, Z., Jiang, B., Zhang, Q.: Robust decentralised load frequency control for interconnected time delay power systems using sliding mode techniques. IET Control Theory Appl. 14(3), 470–480 (2020)
6. Nosratabadi, S.M., Bornapour, M., Gharaei, M.A.: Grasshopper optimization algorithm for optimal load frequency control considering predictive functional modified PID controller in restructured multi-resource multi-area power system with redox flow battery units. Control Eng. Pract. 89, 204–227 (2019)
7. Sharma, G., Krishnan, N., Arya, Y., Panwar, A.: Impact of ultracapacitor and redox flow battery with JAYA optimization for frequency stabilization in linked photovoltaic-thermal system. Int. Trans. Electr. Energy Syst. 31(5), e12883 (2021)
8. Ahmed, M., Magdy, G., Khamies, M., Kamel, S.: Modified TID controller for load frequency control of a two-area interconnected diverse-unit power system. Int. J. Electr. Power Energy Syst. 135, 107528 (2022)
9. Çelik, E., Öztürk, N., Arya, Y., Ocak, C.: (1+ PD)-PID cascade controller design for performance betterment of load frequency control in diverse electric power systems. Neural. Comput. Appl. 33(22), 15433–15456 (2021)
10. Sahoo, G., Sahu, R.K., Panda, S., Samal, N.R., Arya, Y.: Modified Harris Hawks optimization-based fractional-order fuzzy PID controller for frequency regulation of multi-micro-grid. Arab. J. Sci. Eng. 1–25 (2023)
11. Singh, K., Arya, Y.: Tidal turbine support in microgrid frequency regulation through novel cascade fuzzy-FOPID droop in de-loaded region. ISA Trans. 133, 218–232 (2023)
12. Irudayaraj, A.X.R., Wahab, N.I.A., Umamaheswari, M.G., Radzi, M.A.M., Sulaiman, N.B., Veerasamy, V., et al.: A Matignon's theorem based stability analysis of hybrid power system for automatic load frequency control using atom search optimized FOPID controller. IEEE Access 8, 168751–168772 (2020)
13. Veerasamy, V., Wahab, N.I.A., Ramachandran, R., Othman, M.L., Hizam, H., Irudayaraj, A.X.R., et al.: A Hankel matrix based reduced order model for stability analysis of hybrid power system using PSO-GSA optimized cascade PI-PD controller for automatic load frequency control. IEEE Access 8, 71422–71446 (2020)
14. Pappachen, A., Fathima, A.P.: Critical research areas on load frequency control issues in a deregulated power system: a state-of-the-art-of-review. Renewable Sustainable Energy Rev. 72, 163–177 (2017)
15. Shankar, R., Pradhan, S., Chatterjee, K., Mandal, R.: A comprehensive state of the art literature survey on LFC mechanism for power system. Renewable Sustainable Energy Rev. 76, 1185–1207 (2017)
16. Alhelou, H.H., Hamedani-Golshan, M.E., Zamani, R., Heydarian-Forushani, E., Siano, P.: Challenges and opportunities of load frequency control in conventional, modern and future smart power systems: a comprehensive review. Energies 11(10), 2497 (2018)
17. Peddakapu, K., Mohamed, M., Srinivasarao, P., Arya, Y., Leung, P., Kishore, D.: A state-of-the-art review on modern and future developments of AGC/LFC of conventional and renewable energy-based power systems. Renewable Energy Focus 43, 146–171 (2022)
18. Darvish Falehi, A.: Optimal fractional order BELBIC to ameliorate small signal stability of interconnected hybrid power system. Environ. Prog. Sustainable Energy 38(5), 13208 (2019)
19. Darvish Falehi, A.: Robust and intelligent type-2 fuzzy fractional-order controller-based automatic generation control to enhance the damping performance of multi-machine power systems. IETE J. Res. 68(4), 2548–2559 (2022)
20. Falehi, A.D.: MOBA based design of FOPID-SSSC for load frequency control of interconnected multi-area power systems. Smart Struct. Syst. 22(1), 81–94 (2018)
21. Eke, I., Saka, M., Gozde, H., Arya, Y., Taplamacioglu, M.C.: Heuristic optimization based dynamic weighted state feedback approach for 2DOF PI-controller in automatic voltage regulator. Eng. Sci. Technol., Int. J. 24(4), 899–910 (2021)
22. Ali, S.W., Verma, A.K., Terriche, Y., Sadiq, M., Su, C.L., Lee, C.H., et al.: Finite-control-set model predictive control for low-voltage-ride-through enhancement of PMSG based wind energy grid connection systems. Mathematics. 10(22), 4266 (2022)
23. Ismail, M.M., Bendary, A.F., Elsisi, M.: Optimal design of battery charge management controller for hybrid system PV/wind cell with storage battery. Int. J. Power Energy Convers. 11(4), 412–429 (2020)
24. Elsisi, M.: New design of adaptive model predictive control for energy conversion system with wind torque effect. J. Cleaner Prod. 240, 118265 (2019)
25. Mohamed, M.A.E., Mohamed, S.M.R., Saied, E.M.M., Elsisi, M., Su, C.L., Hadi, H.A.: Optimal energy management solutions using artificial intelligence techniques for photovoltaic empowered water desalination plants under cost function uncertainties. IEEE Access 10, 93646–93658 (2022)
26. Sadiq, M., Aragon, C.A., Terriche, Y., Ali, S.W., Su, C.L., Buzna, L., et al.: Continuous-control-set model predictive control for three-level

DC–DC converter with unbalanced loads in bipolar electric vehicle charging stations. Mathematics 10(19), 3444 (2022)
27. Ali, M.N., Soliman, M., Ebrahim, M.A., Elsisi, M.: D-decomposition-based multi-objective robust resilient control for blade pitch of wind energy conversion system. Int. J. Electr. Power Energy Syst. 146, 108781 (2023)
28. Patel, V., Guha, D., Purwar, S.: Frequency regulation of nonlinear power systems using neural network observer-based optimized resilient controller. Int. Trans. Electr. Energy Syst. 2022, 6286500 (2022)
29. Hashim, F.A., Houssein, E.H., Hussain, K., Mabrouk, M.S., Al-Atabany, W.: Honey badger algorithm: new metaheuristic algorithm for solving optimization problems. Math. Comput. Simul 192, 84–110 (2022)
30. El-Bahay, M.H., Lotfy, M.E., El-Hameed, M.A.: Effective participation of wind turbines in frequency control of a two-area power system using coot optimization. Prot. Control Mod. Power Syst. 8(1), 1–15 (2023)
31. Khadanga, R.K., Nayak, S.R., Panda, S., Das, D., Prusty, B.R., Sahu, P.R., et al.: A novel optimal robust design method for frequency regulation of three-area hybrid power system utilizing honey badger algorithm. Int. Trans. Electr. Energy Syst. 2022, 6017066 (2022)
32. Ozumcan, S., Ozturk, A., Varan, M., Andic, C.: A novel honey badger algorithm based load frequency controller design of a two-area system with renewable energy sources. Energy Rep. 9, 272–279 (2023)
33. Brijet, Z., Suresh, T.: Optimum control of under-grate pressure of clinker cooler by optimizing the proportional integral derivative controller parameters using honey badger algorithm technique. Optim. Control Appl. Methods 44(5), 2938–2959 (2023)
34. Bouguenna, I.F., Azaiz, A., Tahour, A., Larbaoui, A.: Robust neuro-fuzzy sliding mode control with extended state observer for an electric drive system. Energy 169, 1054–1063 (2019)
35. Sun, H., Hou, L., Zong, G., Guo, L.: Composite anti-disturbance attitude and vibration control for flexible spacecraft. IET Control Theory Appl. 11(14), 2383–2390 (2017)
36. Tran, A.T., Le Ngoc Minh, B., Tran, P.T., Huynh, V.V., Phan, V.D., Pham, V.T., et al.: Adaptive integral second-order sliding mode control design for load frequency control of large-scale power system with communication delays. Complexity. 2021, 5564184 (2021)
37. Liao, K., Xu, Y.: A robust load frequency control scheme for power systems based on second-order sliding mode and extended disturbance observer. IEEE Trans. Ind. Inf. 14(7), 3076–3086 (2017)
38. Lai, B.H., Tran, A.T., Pham, N.T., Van Huynh, V.: Sliding mode load frequency regulator for different-area power systems with communication delays. J. Adv. Eng. Comput. 5(2), 93–107 (2021)
39. Mi, Y., He, X., Hao, X., Li, Z., Fu, Y., Wang, C., et al.: Frequency control strategy of multi-area hybrid power system based on frequency division and sliding mode algorithm. IET Gener. Transm. Distrib. 13(7), 1145–1152 (2019)
40. Dev, A., Sarkar, M.K.: Robust higher order observer based non-linear super twisting load frequency control for multi area power systems via sliding mode. Int. J. Control Autom. Syst. 17(7), 1814–1825 (2019)
41. Mi, Y., Fu, Y., Wang, C., Wang, P.: Decentralized sliding mode load frequency control for multi-area power systems. IEEE Trans. Power Syst. 28(4), 4301–4309 (2013)
42. Sarkar, M.K., Dev, A., Asthana, P., Narzary, D.: Chattering free robust adaptive integral higher order sliding mode control for load frequency problems in multi-area power systems. IET Control Theory Appl. 12(9), 1216–1227 (2018)
43. Prasad, S., Purwar, S., Kishor, N.: Load frequency regulation using observer based non-linear sliding mode control. Int. J. Electr. Power Energy Syst. 104, 178–193 (2019)
44. Tran, A.T., Minh, B.L.N., Huynh, V.V., Tran, P.T., Amaefule, E.N., Phan, V.D., et al.: Load frequency regulator in interconnected power system using second-order sliding mode control combined with state estimator. Energies 14(4), 863 (2021)
45. Alyoussef, F., Kaya, I.: Improved adaptive dynamic non-singular terminal sliding mode controller with fractional disturbance observer. Inf. Sci. 641, 119110 (2023)
46. Tran, A.T., Pham, N.T., Van Huynh, V., Dang, D.N.M.: Stabilizing and enhancing frequency control of power system using decentralized observer-based sliding mode control. J. Control Autom. Electr. Syst. 34(3), 541–553 (2023)
47. Patel, V., Guha, D., Purwar, S.: Minimum order disturbance observer-aided integral sliding mode controller for frequency regulation of hybrid power system. In: Control of Standalone Microgrid, pp. 277–296. Elsevier, New York (2021)
48. Yang, F., Shao, X., Muyeen, S., Li, D., Lin, S., Fang, C.: Disturbance observer based fractional-order integral sliding mode frequency control strategy for interconnected power system. IEEE Trans. Power Syst. 36(6), 5922–5932 (2021)
49. Guha, D., Roy, P.K., Banerjee, S.: Adaptive fractional-order sliding-mode disturbance observer-based robust theoretical frequency controller applied to hybrid wind–diesel power system. ISA Trans. 133, 160–183 (2022)
50. Mu, C., Tang, Y., He, H.: Improved sliding mode design for load frequency control of power system integrated an adaptive learning strategy. IEEE Trans. Ind. Electron. 64(8), 6742–6751 (2017)
51. Khooban, M.H.: Secondary load frequency control of time-delay stand-alone microgrids with electric vehicles. IEEE Trans. Ind. Electron. 65(9), 7416–7422 (2017)
52. Shouran, M., Anayi, F., Packianather, M.: Design of sliding mode control optimised by the Bees algorithm for LFC in the Great Britain power system. Mater. Today:. Proc. 52(3), 937–943 (2021)
53. Kumar, A., Anwar, M.N., Kumar, S.: Sliding mode controller design for frequency regulation in an interconnected power system. Prot. Control Mod. Power Syst. 6(1), 1–12 (2021)
54. Zhang, C.L., Wu, X.Z., Xu, J.: Particle swarm sliding mode-fuzzy PID control based on maglev system. IEEE Access 9, 96337–96344 (2021)
55. Kennedy, J., Eberhart, R.: Particle swarm optimization. In: Proceedings of ICNN'95-International Conference on Neural Networks, 1942–1948. IEEE, Piscataway, NJ (1995)
56. Xie, L., Han, T., Zhou, H., Zhang, Z.R., Han, B., Tang, A.: Tuna swarm optimization: a novel swarm-based metaheuristic algorithm for global optimization. Comput. Intell. Neurosci. 2021, 1–22 (2021)
57. Huynh, V.V., Tran, P.T., Minh, B.L.N., Tran, A.T., Tuan, D.H., Nguyen, T.M., et al.: New second-order sliding mode control design for load frequency control of a power system. Energies 13(24), 6509 (2020)
58. Fu, C., Wang, C., Shi, D., et al.: An alternative method for mitigating impacts of communication delay on load frequency control. Int. J. Electr. Power Energy Syst. 119, 105924 (2020)
59. Katsuhiko, O.: Modern Control Engineering. Prentice-Hall, Hoboken, NJ (2010)

How to cite this article: Tran, A.-T., Duong, M.P., Pham, N.T., Shim, J.W.: Enhanced sliding mode controller design via meta-heuristic algorithm for robust and stable load frequency control in multi-area power systems. IET Gener. Transm. Distrib. 18, 460–478 (2024). https://doi.org/10.1049/gtd2.13077